

# CCPG1 recognizes endoplasmic reticulum luminal proteins for selective ER-phagy

Shunsuke Ishii<sup>a,†</sup>, Haruka Chino<sup>b,†,‡</sup>, Koji L. Ode<sup>c</sup>, Yoshitaka Kurikawa<sup>b</sup>, Hiroki R. Ueda<sup>c,d</sup>, Akira Matsuura<sup>e</sup>, Noboru Mizushima<sup>b,\*</sup>, and Eisuke Itakura<sup>e,\*</sup>

<sup>a</sup>Department of Biology, Graduate School of Science and Engineering, Chiba University, Chiba 263-8522, Japan;

<sup>b</sup>Department of Biochemistry and Molecular Biology, Graduate School of Medicine, Tokyo 113-0033, Japan;

<sup>c</sup>Department of Systems Pharmacology, Graduate School of Medicine, University of Tokyo, Tokyo 113-0033, Japan;

<sup>d</sup>Laboratory for Synthetic Biology, RIKEN Center for Biosystems Dynamics Research, Osaka 565-0871, Japan;

<sup>e</sup>Department of Biology, Graduate School of Science, Chiba University, Chiba, 263-8522, Japan

**ABSTRACT** The endoplasmic reticulum (ER) is a major cell compartment where protein synthesis, folding, and posttranslational modifications occur with assistance from a wide variety of chaperones and enzymes. Quality control systems selectively eliminate abnormal proteins that accumulate inside the ER due to cellular stresses. ER-phagy, that is, selective autophagy of the ER, is a mechanism that maintains or reestablishes cellular and ER-specific homeostasis through removal of abnormal proteins. However, how ER luminal proteins are recognized by the ER-phagy machinery remains unclear. Here, we applied the aggregation-prone protein, six-repeated islet amyloid polypeptide (6xIAPP), as a model ER-phagy substrate and found that cell cycle progression 1 (CCPG1), which is an ER-phagy receptor, efficiently mediates its degradation via ER-phagy. We also identified prolyl 3-hydroxylase family member 4 (P3H4) as an endogenous cargo of CCPG1-dependent ER-phagy. The ER luminal region of CCPG1 contains several highly conserved regions that we refer to as cargo-interacting regions (CIRs); these interact directly with specific luminal cargos for ER-phagy. Notably, 6xIAPP and P3H4 interact directly with different CIRs. These findings indicate that CCPG1 is a bispecific ER-phagy receptor for ER luminal proteins and the autophagosomal membrane that contributes to the efficient removal of aberrant ER-resident proteins through ER-phagy.

## Monitoring Editor

Sharon Tooze

The Francis Crick Institute

Received: Sep 26, 2022

Revised: Dec 23, 2022

Accepted: Jan 27, 2023

This article was published online ahead of print in MBoC in Press (<http://www.molbiolcell.org/cgi/doi/10.1091/mbc.E22-09-0432>) on February 3, 2023.

<sup>†</sup>These authors contributed equally to this work.

<sup>\*</sup>Present address: Department of Cell Biology, Harvard Medical School, Boston, MA 02115.

Author contributions: S.I. and H.C. performed the experiments; K.L.O. performed mass spectrometry under the supervision of H.R.U.; Y.K. provided experimental support; A.M. contributed to the writing and data interpretation; S.I., H. C., N. M., and E.I. conceptualized the project and wrote the manuscript.

Conflict of interest: The authors declare no conflicts of interest.

<sup>\*</sup>Address correspondence to: Eisuke Itakura ([eitakura@chiba-u.jp](mailto:eitakura@chiba-u.jp)); Noboru Mizushima ([nmizu@m.u-tokyo.ac.jp](mailto:nmizu@m.u-tokyo.ac.jp)).

Abbreviations used: ATG, autophagy-related; CCPG1, cell cycle progression 1; CIR, cargo-interacting region; FIR, FIP200-interacting region; IAPP, islet amyloid polypeptide; LIR, LC3-interacting region; P3H4, prolyl 3-hydroxylase family member 4; RG, RFP-GFP; WT, wild type.

© 2023 Ishii et al. This article is distributed by The American Society for Cell Biology under license from the author(s). Two months after publication it is available to the public under an Attribution-NonCommercial-Share Alike 4.0 International Creative Commons License (<http://creativecommons.org/licenses/by-nc-sa/4.0>).

"ASCB®," "The American Society for Cell Biology®," and "Molecular Biology of the Cell®" are registered trademarks of The American Society for Cell Biology.

## INTRODUCTION

The endoplasmic reticulum (ER) is the largest organelle and synthesizes approximately 35% of the proteins in a cell (Uhlén et al., 2015; Juszkievicz and Hegde, 2018). These proteins mature through processes occurring in the ER, including cleavage of signal sequences, folding, disulfide bond formation, and glycosylation. Then the proteins are selectively transported to the endomembrane system, the plasma membrane, or the exterior of the cell (Ellgaard and Helenius, 2003; Bukau et al., 2006; Ni and Lee, 2007). However, external stresses and genetic mutations can lead to the accumulation of unfolded proteins in the ER, causing ER storage diseases (e.g., hereditary emphysema; Callea et al., 1992; Rutishauser and Spiess, 2002; Hebert and Molinari, 2007). Unfolded proteins accumulated in the ER are recognized by unfolded protein response (UPR) receptors (IRE1, PERK, and ATF6), which induce molecular chaperones to re-fold or degrade the proteins through ER-associated degradation (ERAD); this is known as the ER stress response pathway (Chakrabarti et al., 2011; Ruggiano et al., 2014; Hetz et al., 2020). However, not

all misfolded proteins in the ER are degraded through ERAD (Houck *et al.*, 2014; De Leonibus *et al.*, 2019).

Macroautophagy (hereafter referred to as autophagy) is a bulk degradation system in which an isolation membrane engulfs a portion of the cytoplasm and delivers it to lysosomes for degradation (Mizushima and Komatsu, 2011; Mercer *et al.*, 2018; Melia *et al.*, 2020; Klionsky *et al.*, 2021). Recent studies have revealed that large cellular structures, such as organelles (Lemasters, 2005; Singh *et al.*, 2009; Maejima *et al.*, 2013), ribosomes (Kraft *et al.*, 2008), protein aggregates (Webb *et al.*, 2003; Øverbye *et al.*, 2007), invading pathogens (Nakagawa *et al.*, 2004), lysosomes (Maejima *et al.*, 2013) and protein droplets (Wilfling *et al.*, 2020; Yamasaki *et al.*, 2020), are selectively degraded via autophagy. This selectivity is achieved through autophagy receptors, which link cargos to the autophagosomal membrane. The interaction motifs between autophagy receptors and autophagy-related gene (ATG) proteins are evolutionarily conserved, as several proteins contain the microtubule-associated protein light chain 3 (LC3)-interacting region (LIR). The LIR contributes to selective interaction with cargos, which are recruited to the autophagosomal membrane (Stolz *et al.*, 2014). The FIP200-interacting region (FIR) is another binding motif that links cargos to FIP200, a component of the ULK1 complex that is indispensable to autophagy induction (Smith *et al.*, 2018; Turco *et al.*, 2019). ER-phagy (reticulophagy) is a type of autophagy that can selectively remove the ER (De Duve, 1963; Bernales *et al.*, 2006) and maintains ER homeostasis through remodeling of ER conformation via the degradation of excessive membrane or removal of unfolded luminal proteins (Jia *et al.*, 2011; Pengo *et al.*, 2013; Molinari, 2021).

Since the identification of yeast ATG39 and ATG40, as well as mammalian FAM134B, as ER-phagy receptors (Khaminets *et al.*, 2015; Mochida *et al.*, 2015), several additional ER-phagy receptor proteins have been identified, including SEC62 (Fumagalli *et al.*, 2016), RTN3L (Grumati *et al.*, 2017), cell cycle progression 1 (CCPG1) (Smith *et al.*, 2018), TEX264 (An *et al.*, 2019; Chino *et al.*, 2019), ATL3 (Chen *et al.*, 2019), CALCOCO1 (Nthiga *et al.*, 2020), C53 (Stephani *et al.*, 2020), Epr1 (Zhao *et al.*, 2020), and RHD3 (Sun *et al.*, 2022). All ER-phagy receptors tether the ER membrane to the autophagosomal membrane through interaction with Atg8/LC3 (Mochida and Nakatogawa, 2022). CCPG1 also interacts with FIP200 (Smith *et al.*, 2018). Each receptor is responsive to diverse intracellular stresses. The reticulon-like proteins ATG40 and FAM134B have short hairpin transmembrane domains and generate membrane curvature, leading to fragmentation of the ER and incorporation into the autophagosome under starvation conditions (Bhaskara *et al.*, 2019; Jiang *et al.*, 2020; Mochida *et al.*, 2020). SEC62 causes ER degradation during recovery from ER stress (Fumagalli *et al.*, 2016), while CCPG1 promotes peripheral ER degradation during ER stress (Smith *et al.*, 2018). TEX264 ensures the canonical degradation of the ER via ER-phagy and is regulated by phosphorylation of its LIR (Chino *et al.*, 2019, 2022). SEC62, CCPG1, and TEX264 all have one or two transmembrane domains, and only CCPG1 has a long intraluminal domain.

In the UPR pathway, luminal domains of UPR receptors on the ER membrane sense unfolded luminal proteins in the ER and activate UPR signaling (Schröder and Kaufman, 2005). Although bulk incorporation of the ER into autophagosomes via ER-phagy receptors has been studied thoroughly, the process of selective protein recognition inside the ER during ER-phagy remains largely unexplored. Recent studies have revealed that several ER-resident proteins link ER-luminal cargos to ER-phagy receptors. Calnexin and binding immunoglobulin protein (BiP) are ER chaperones that deliver misfolded proteins to the ERAD machinery and also interact with

FAM134B to mediate ER-phagy for misfolded procollagen (Fregno *et al.*, 2018; Forrester *et al.*, 2019). PGRMC1, which is a binding partner of ER-phagy receptor RTN3L, captures low-molecular-weight misfolded proteins (Chen *et al.*, 2021). However, whether any of these ER-phagy receptors can directly recognize ER luminal proteins for selective ER-phagy remains unclear.

In this study, we characterized an ER luminal protein, six-repeated islet amyloid polypeptide (6xIAPP), as a model ER-phagy substrate in mammalian cells and found that aggregated 6xIAPP is efficiently degraded by ATG protein- and CCPG1-dependent ER-phagy processes. We found that the luminal region of CCPG1 is essential for ER-phagic degradation of selective proteins and identified prolyl 3-hydroxylase family member 4 (P3H4) as an endogenous ER luminal protein recognized by CCPG1. CCPG1 possesses several highly conserved regions among vertebrates, and 6xIAPP and P3H4 interact directly with different parts of the luminal CCPG1 domains, which contain cargo-interacting regions (CIRs). Thus, our data revealed that CCPG1 luminal regions directly recognize ER luminal cargos for ER-phagy, and simultaneous binding of multiple cargos to CCPG1 might drive the efficient removal of aberrant ER-resident proteins.

## RESULTS

### 6xIAPP-RFP-GFP-KDEL is delivered to the lysosomes

Islet amyloid polypeptide (IAPP) is a 37-amino acid (aa) protein secreted from pancreatic islet  $\beta$ -cells, and aggregation of IAPP is associated with type 2 diabetes (Klöppel *et al.*, 1985; Butler *et al.*, 2003). As 6xIAPP forms oligomers and induces severe ER stress in yeast (Kayatekin *et al.*, 2018), we examined whether 6xIAPP is degraded through ER-phagy in mammalian cells. To monitor lysosomal degradation of IAPP, 6xIAPP or 1xIAPP was fused with red fluorescent protein (RFP), green fluorescent protein (GFP), and an ER retention signal, KDEL (forming IAPP-RFP-GFP-KDEL, hereafter referred to as IAPP-RG) and inserted into a lentivirus vector under a doxycycline (Dox)-dependent promoter (Figure 1A). In mammalian cells, 6xIAPP-RG showed reticular and dotlike localization patterns and increased molecular mass, compared with 1xIAPP-RG, which was similar in size to the 4.3-MDa ribosome complex (60S ribosome protein L19; RPL19) (Supplemental Figure S1, A and B). Glycosylation can be an indicator of proteins translocated into the ER lumen. Because IAPP-RG does not have any glycosylation sites, its electrophoretic mobility was not altered by treatment with endoglycosidase H (Endo H; Supplemental Figure S1C). Therefore, we artificially inserted an opsin glycosylation site into the C-terminus of each IAPP construct (IAPP-Gly-HA-KDEL and IAPP-RG-Gly-KDEL). These proteins (both 1x and 6xIAPP) underwent glycosylation in mammalian cells (Supplemental Figure S1, D–G). Membrane permeabilization assays also showed that, while cytosol-facing RFP-GFP-cytochrome b5 (RG-Cytb5; a transmembrane domain of cytochrome b5 fused with RFP-GFP) was readily stained with anti-GFP antibody after digitonin treatment, 6xIAPP-RG was stained only after cells had been treated with the stronger detergent Triton X-100 but not digitonin (Supplemental Figure S1H). These results suggest that 6xIAPP in mammalian cells primarily resides in the ER luminal environment at steady state.

When IAPP-RG is delivered to the lysosomes, the acidic conditions and lysosomal proteases rapidly attenuate GFP fluorescence. In contrast, RFP, which is relatively resistant to the lysosomal environment, accumulates within the lysosomes (Katayama *et al.*, 2008). Therefore, an increase in the RFP signal of lysosomes detected through fluorescence microscopy, elevation of the RFP/GFP ratio based on flow cytometry, and detection of cleaved RFP through

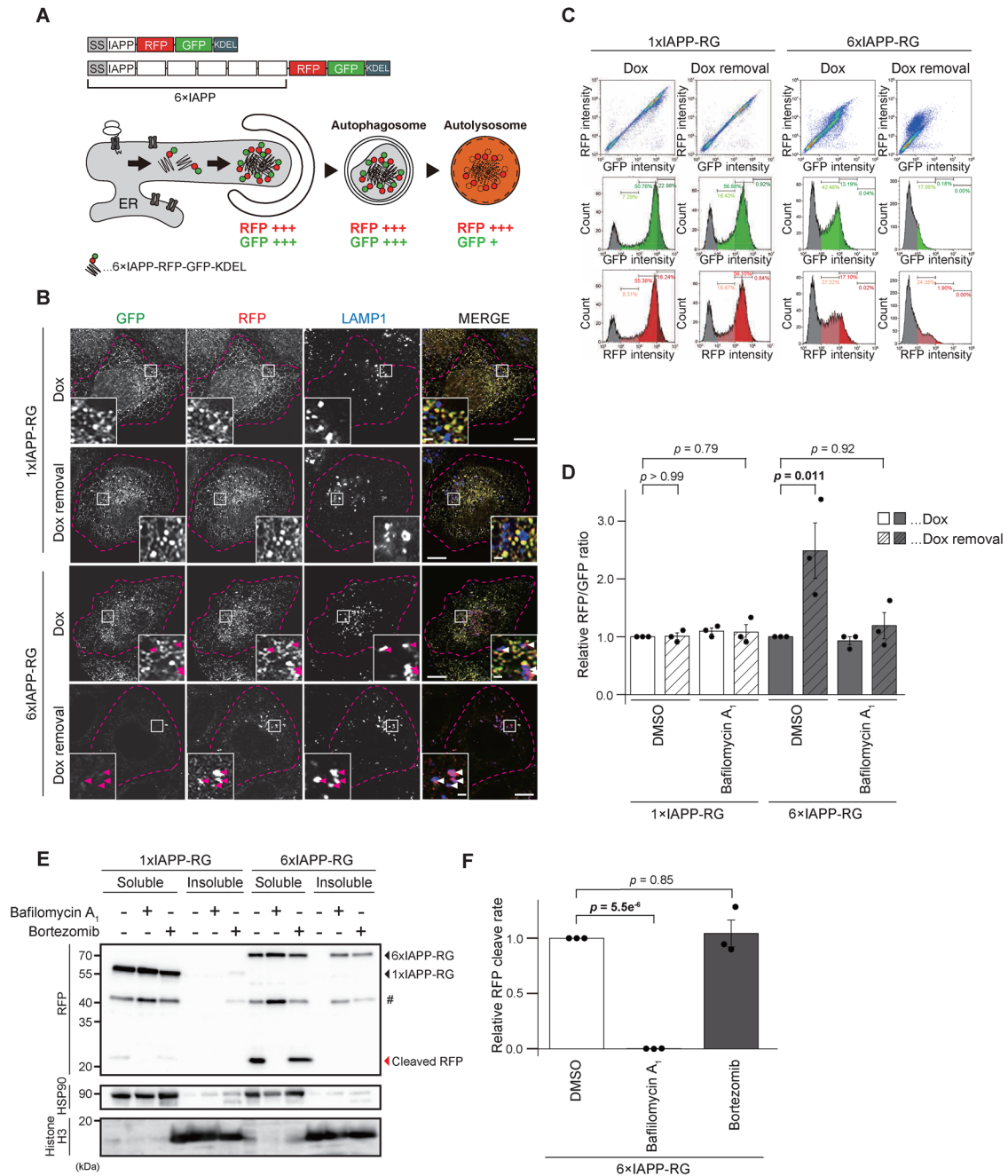


**FIGURE 1:** 6xIAPP-RFP-GFP-KDEL is delivered to lysosomes. (A) Schematic diagrams of the ER-phagy substrate 1x (or 6x) IAPP-RFP-GFP-KDEL (1x or [6x] IAPP-RG). In the lysosome, GFP fluorescence is diminished, whereas RFP fluorescence remains intact due to resistance to acidic pH and lysosomal proteases. (B–D) 6xIAPP, but not 1xIAPP, is delivered to lysosomes. Tet-On HeLa cells expressing 1x (or 6x) IAPP-RG were incubated in medium containing doxycycline (Dox) for 24 h and then cultured in medium with or without Dox for a further 24 h. After fixation, the cells were stained with antibodies against LAMP1 and analyzed by confocal microscopy. GFP-negative and RFP-positive signals accumulated in LAMP1-positive structures (arrowhead) are indicated. Scale bars represent 10 and 1  $\mu$ m (inset) (B). The cells treated with Dox as described above were trypsinized, and their green and red fluorescence intensities were measured using flow cytometry. Representative dot plots of GFP versus RFP intensities and corresponding histograms are shown, C. The fluorescence ratio was calculated in RFP-positive cells. Data represent the mean  $\pm$  standard error (SE) of at least three independent experiments. Differences were statistically analyzed by Dunnett's multiple comparison test, D. (E, F) Proteasomal inhibition is not related to lysosomal degradation of 6xIAPP. Tet-On HeLa cells expressing 1x (or 6x) IAPP-RG were cultured in medium containing Dox with dimethylsulfoxide (DMSO), bafilomycin A<sub>1</sub>, or bortezomib for 24 h before immunoblotting analysis using antibodies against RFP, HSP90, and Histone H3. Cell lysates were centrifuged, and the supernatants were collected as the soluble fraction. The pellets containing the nuclear compartment were collected as the insoluble fraction. Each pellet was resuspended in an equal volume of lysis buffer. # indicates degradative products of IAPP-RG, E. The band intensities of cleaved RFP and 6xIAPP-RG were quantified, and the ratio of cleaved RFP/total amount of 6xIAPP (normalized to DMSO treatment) is shown. Data represent the mean  $\pm$  SE of three independent experiments. Differences were statistically analyzed by Dunnett's multiple comparison test, F.



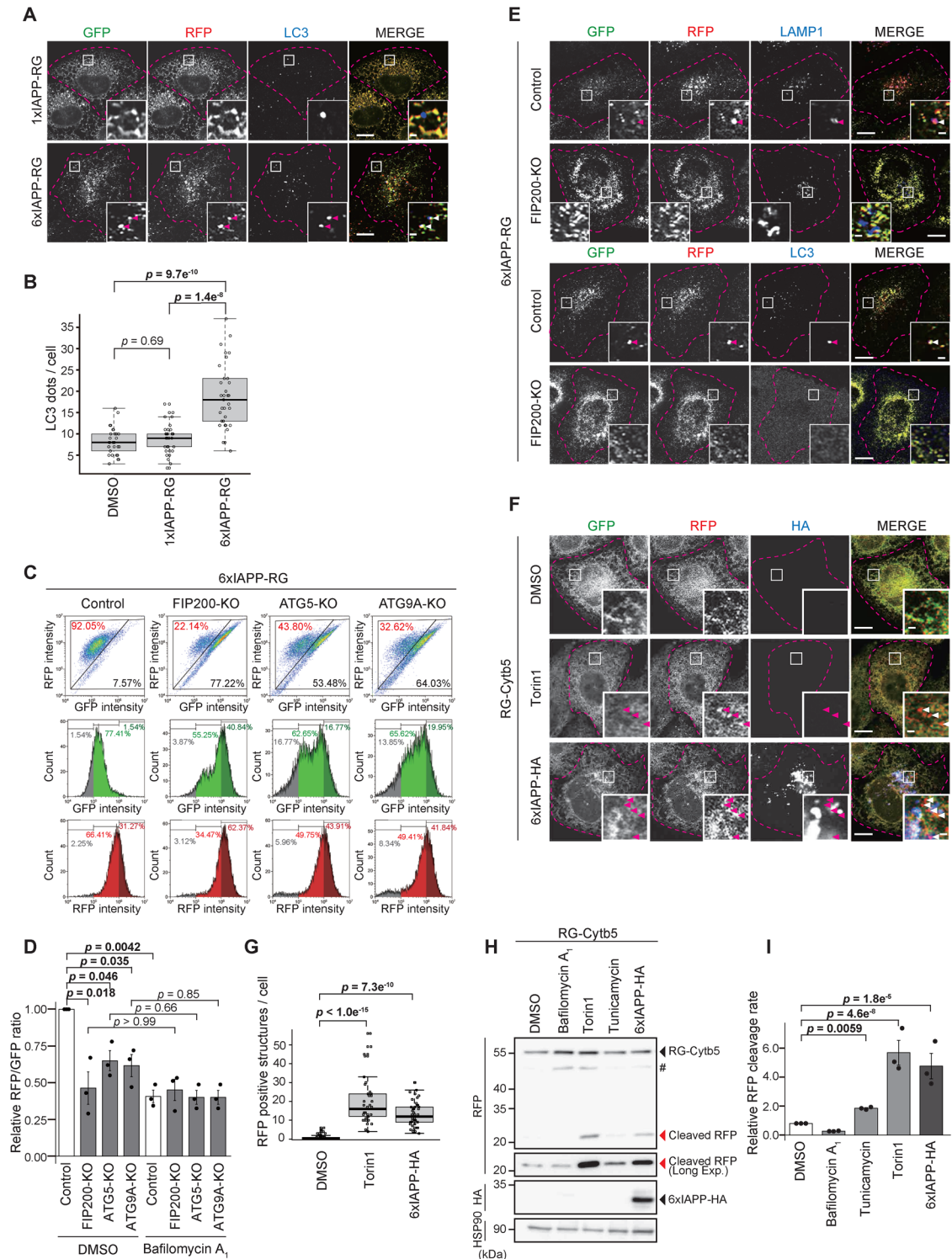


**FIGURE 2: ER-phagy degrades 6xIAPP in the ER.** (A, B) Dot structure of 6xIAPP-RG colocalized with endogenous LC3. Tet-On HeLa cells expressing 1x (or 6x) IAPP-RG were incubated in medium containing Dox for 48 h before fixation. The cells were stained with antibodies against LC3 and analyzed through confocal microscopy. Scale bars represent 10 and 1  $\mu$ m (inset), A. Quantification of the number of LC3 puncta per cell. Solid bars indicate the median, boxes the interquartile range (25th–75th percentile), and whiskers the 0th–100th percentile range. Data were collected from 33 cells of each cell type. Differences were analyzed using one-way analysis of variance (ANOVA) and Sidak’s multiple comparison test, B. (C–E) 6xIAPP-RG accumulated in autophagy-KO cells. Tet-On HeLa cells stably expressing Cas9 and the indicated sgRNA were cultured in the presence of Dox for 24 h (a mixed population of wild-type [WT] and knockout [KO] cells was used). Following the removal of Dox, the cells were cultured with or without bafilomycin A<sub>1</sub> for 24 h before flow cytometry. Dot plots of GFP versus RFP fluorescence intensities are shown, with black letters indicating the lysosomal fraction (%) and red letters all other fractions (%), C. The fluorescence ratio was calculated for RFP-positive cells. Data represent the mean  $\pm$  SE of three independent experiments. Differences were analyzed using one-way



immunoblotting can be interpreted as representing lysosomal degradation of IAPP-RG.

1xIAPP-RG was clearly colocalized with translocon-associated protein subunit alpha (TRAP $\alpha$ ), which is an ER marker (Supplemental Figure S1I), but not with lysosomal-associated membrane protein 1 (LAMP1), which is a lysosome marker (Figure 1B). On the other hand, although 6xIAPP-RG showed a reticular pattern and numerous dot structures colocalized with the TRAP $\alpha$  signal, GFP-negative and RFP-positive signals of 6xIAPP-RG accumulated in LAMP1-positive lysosomes, and RFP signals associated with lysosomes remained after Dox removal (Figure 1B and Supplemental Figure S1I). We next quantified the reduction in fluorescence after Dox removal through flow cytometry. Although 1xIAPP-RG was stable, 6xIAPP-RG was rapidly degraded within 24 h of Dox removal (Figure 1C). Notably, the RFP/GFP ratio of 6xIAPP-RG was efficiently increased to 2.5-fold higher than that of 1xIAPP-RG (Figure 1, C and D), and this increase was clearly suppressed by the lysosomal inhibitor bafilomycin A<sub>1</sub> (Figure 1D; Supplemental Figure S2A). Treatment with bafilomycin A<sub>1</sub> enlarged lysosomes and caused the accumulation of GFP and RFP signals of 6xIAPP-RG, but not 1xIAPP-RG, inside lysosomes (Supplemental Figure S2B). We confirmed that 6xIAPP-HA-KDEL (6xIAPP-HA), in which HA was used instead of RFP-GFP, also accumulated upon bafilomycin A<sub>1</sub> treatment; these findings suggested that lysosomal degradation of 6xIAPP is not mediated by the RFP-GFP tag (Supplemental Figure S2, C and D). Moreover, both 6xIAPP-RG and 6xIAPP-HA accumulated inside lysosomes after the inactivation of lysosomal proteases using a lysosome inhibitor cocktail that contained E64d, pepstatin A, and leupeptin (Supplemental Figure S2E). Flow cytometric analysis also demonstrated a significant reduction in the RFP signal for 6xIAPP-RG. A previous report revealed that 6xIAPP on the ER is degraded by the proteasome in yeast (Kayatekin *et al.*, 2018). Indeed, treatment not only with bafilomycin A<sub>1</sub>, but also with the proteasomal inhibitor bortezomib, led to 6xIAPP-RG accumulation in the insoluble fraction (Figure 1E). Importantly, while bafilomycin A<sub>1</sub> clearly inhibited the generation of cleaved RFP, bortezomib neither reduced nor increased the amount of cleaved RFP derived from 6xIAPP-RG (Figure 1, E and F), indicating that the proteasome system is not associated with lysosomal degradation under these conditions. The 6xIAPP accumulated due to proteasome inhibition is likely located in the cytosol, where it cannot be removed through ER-phagy. We found that both GFP and RFP signals in cells expressing low 6xIAPP-RG levels were diminished after Dox removal. In contrast, only the GFP signal was markedly reduced in cells strongly expressing 6xIAPP-RG (Supplemental Figure S2, F and G). Although most of the 6xIAPP that accumulated under proteasome inhibitor treatment was not glycosylated,

some glycosylated 6xIAPP accumulated under lysosomal inhibitor (Supplemental Figure S2H). These results indicate that 6xIAPP exists in two distinct populations in mammalian cells, undergoing lysosomal and proteasomal degradation, respectively. Cells highly expressing 6xIAPP-RG were used to detect lysosomal degradation in subsequent experiments.

### 6xIAPP in the ER is degraded by ER-phagy

GFP dot structures of 6xIAPP-RG, but not 1xIAPP-RG, were colocalized with LC3, an autophagosome marker (Figure 2A). To verify whether 6xIAPP is degraded by autophagy, HeLa cells expressing 6xIAPP-RG with core autophagy genes knocked out, FIP200 (Hara *et al.*, 2008), ATG5 (Mizushima *et al.*, 2001), or ATG9A (Saitoh *et al.*, 2009), were generated using clustered regularly interspaced short palindromic repeats (CRISPR). Quantitative analysis via flow cytometry revealed that the reduction of GFP signals of 6xIAPP-RG after Dox removal was significantly suppressed in the autophagy-KO cells (Figure 2, C and D; Supplemental Figure S3A). Furthermore, FIP200-KO cells showed diminished colocalization of 6xIAPP-RG with LC3 and fewer RFP dots with LAMP1-positive structures (Figure 2E). These data suggest that 6xIAPP is degraded in an autophagy-dependent manner.

We observed that the number of endogenous LC3 dots was increased when 6xIAPP-RG was expressed (Figure 2, A and B). To quantify autophagic activity, 1x or 6xIAPP-HA under the Tet-On promoter was introduced into HeLa cells stably expressing RFP-GFP-LC3 as a ratiometric autophagy probe (Kimura *et al.*, 2007). With the expression of 6xIAPP-HA, but not 1xIAPP-HA, the RFP/GFP ratio of RFP-GFP-LC3 was elevated 2.7-fold and increased numbers of GFP punctate structures were observed within 48 h of Dox induction (Supplemental Figure S3, B–D). In addition, the amount of endogenous LC3-II increased with expression of the 6xIAPP construct (Supplemental Figure S3, E and F). These data suggest that autophagic activity is promoted by the expression of 6xIAPP.

If ER-phagy degraded 6xIAPP present in the ER lumen, 6xIAPP should be degraded along with ER membrane components. Therefore, we detected the lysosomal degradation of an ER component using RG-Cytb5, which localizes RFP-GFP on the ER (Supplemental Figure S3G). RG-Cytb5 was stably localized to the ER in HeLa cells, and treatment with Torin 1, an inhibitor of mammalian target of rapamycin complex 1 (mTORC1), induced GFP-negative and RFP-positive dots (Figure 2, F and G). The expression of 6xIAPP-HA increased the number of GFP-negative and RFP-positive dots. While tunicamycin, an ER stressor, moderately increased the amount of cleaved RFP, Torin 1 and 6xIAPP-HA induced marked accumulation of cleaved RFP (Figure 2, H and I), suggesting that 6xIAPP is eliminated by ER-phagy alongside ER components.

ANOVA and Sidak's multiple comparison test, D. HeLa cells stably expressing Cas9 and sgRNA for FIP200 or nontarget (control) sgRNA were treated with Dox for 24 h to induce expression of 6xIAPP-RG before fixation. Cells were stained with antibodies against LAMP1 or LC3 and analyzed through immunofluorescence microscopy. Scale bars represent 10 and 1  $\mu$ m (inset), E. (F–I) 6xIAPP induces lysosomal degradation of an ER protein. HeLa cells stably expressing RFP-GFP-cytochrome b5 (RG-Cytb5) were incubated with Dox to induce 6xIAPP-HA-KDEL (6xIAPP-HA) expression, or with Torin 1, for 24 h. After fixation, cells were stained with antibodies against HA and analyzed through immunofluorescence microscopy. GFP-negative and RFP-positive signals (arrowhead) are indicated. Scale bars represent 10 and 1  $\mu$ m (inset), F. Quantification of the number of GFP negative, RFP positive puncta per cell. Solid bars indicate the median, boxes the interquartile range (25th–75th percentile), and whiskers the 0th–100th percentile range. Data were collected from 45 cells of each cell type. Differences were statistically analyzed by Dunnett's multiple comparison test, G. HeLa cells stably expressing RG-Cytb5 were treated with the indicated compounds or Dox for induction of 6xIAPP-HA expression for 24 h. Cell lysates were analyzed through immunoblotting using antibodies against RFP, HA, or endogenous HSP90 (loading control). # indicates degradative products of RG-Cytb5, H. The cleaved RFP/RG-Cytb5 band intensity ratio (normalized to the WT) is shown. Data represent the mean  $\pm$  SE of three independent experiments. Differences were statistically analyzed by Dunnett's multiple comparison test, I.

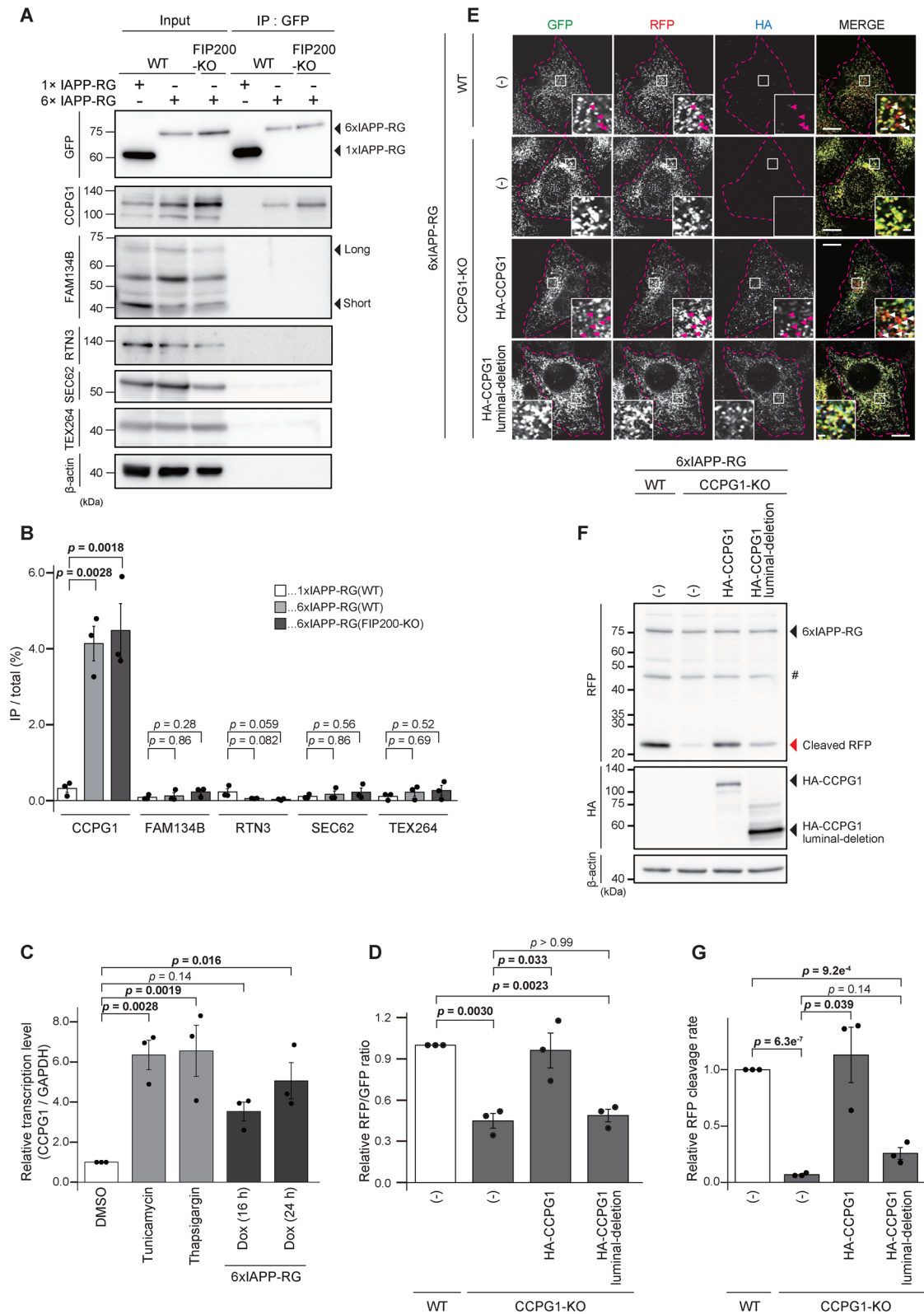


**FIGURE 3:** CCPG1 is an essential ER-phagy receptor for the degradation of 6 × IAPP. (A, B) 6xIAPP-RG selectively interacts with CCPG1 in mammalian cells. Tet-On HeLa cells (WT and FIP200-KO) expressing 1x (or 6x) IAPP-RG were cultured with Dox for 48 h before IP. Inputs (5% of total) and immunoprecipitants (80% of total) were analyzed through immunoblotting using the indicated antibodies, A. The IP product/input ratio is shown. Data represent the mean ± SE of three independent experiments. Differences were statistically analyzed by Dunnett's multiple comparison test, B. (C) The expression of 6xIAPP promotes transcription of CCPG1. Tet-On HeLa cells highly expressing 6xIAPP-RG were treated with each of the ER stressors for 16 h, or Dox to induce 6xIAPP-RG for 16–24 h. Quantitative real-time PCR was performed for endogenous CCPG1 and GAPDH (loading control). Data represent the mean ± SE of three independent

## CCPG1 is the essential ER-phagy receptor associated with the degradation of 6xIAPP

To investigate whether autophagic degradation of 6xIAPP requires ER-phagy receptor proteins, such as FAM134B, SEC62, RTN3, CCPG1, and TEX264, immunoprecipitation (IP) of 1xIAPP-RG and 6xIAPP-RG was performed. While no ER-phagy receptor was precipitated in the presence of 1xIAPP-RG, 6xIAPP-RG co-precipitated with endogenous CCPG1 (Figure 3, A and B). We observed that the amount of endogenous CCPG1, but not the amount of other ER-phagy receptors, was increased upon expression of 6xIAPP-RG (Figure 3A). The increase in CCPG1 was further augmented by bafilomycin A<sub>1</sub> treatment (Figure S4A). Consistent with the previous finding that ER stressors (e.g., tunicamycin and thapsigargin) transcriptionally activate the expression of CCPG1 (Smith *et al.*, 2018), 6xIAPP-RG increased the mRNA abundance of CCPG1 (Figure 3C), suggesting that aggregated ER-luminal proteins induce CCPG1 expression. Additionally, FIP200-KO cells accumulated CCPG1, which also interacts with 6xIAPP. This result is consistent with the finding that CCPG1-KO cells, but not other ER-phagy receptor-KO cells, suppressed the reduction in GFP fluorescence of 6xIAPP-RG, as measured using flow cytometry (Figure 3D; Supplemental Figure S5, A and B). The autophagic degradation of 6xIAPP-RG was restored by exogenous expression of HA-CCPG1 (Figure 3D), suggesting that the KO phenotype is not an off-target effect of CRISPR. We also showed that 6xIAPP formed large complexes (Supplemental Figure S1A) and endogenous CCPG1 migrated to high-density fractions, which have molecular mass similar to that of 6xIAPP (Supplemental Figure S5, C and D). These results indicate that CCPG1 plays an essential role in ER-phagy-dependent degradation of 6xIAPP aggregates.

CCPG1 is a vertebrate-specific gene and regulates ER-phagy via cytoplasmic N-terminal LIR and FIRs (Smith *et al.*, 2018). Notably, among ER-phagy receptors, only CCPG1 has a large ER luminal region, which consists of >500 aa (Kostenko *et al.*, 2006). However, the physiological function of this luminal domain remains unclear. We hypothesized that the ER luminal region of CCPG1 is associated with the recognition of ER luminal cargos. The CCPG1 $\Delta$ 289–757 mutant lacking the whole ER luminal region (CCPG1 luminal deletion) failed to restore the RFP/GFP ratio of 6xIAPP in CCPG1-KO cells (Figure 3D). CCPG1-KO cells showed fewer GFP-negative and RFP-positive dots for 6xIAPP-RG; these were recovered through re-expression of full-length CCPG1, but not CCPG1 luminal deletion (Figure 3E). We then performed an RFP cleavage assay, which demonstrated that reexpression of full-length CCPG1 restored lysosomal degradation of 6xIAPP-RG (Figure 3, F and G). On the other hand,

reexpression of CCPG1 luminal deletion had only a moderate effect on CCPG1-KO, likely due to bulk ER-phagy via the cytoplasmic domain of CCPG1. These results indicate that the luminal region of CCPG1 is required for ER-phagy-dependent lysosome degradation of 6xIAPP.

Overexpression of CCPG1 leads to the formation of punctate structures on the ER, which reportedly colocalize with ATG proteins in mammalian cells (Smith *et al.*, 2018). Although the luminal-deletion mutant of CCPG1 colocalized with LC3, the rate of puncta formation was reduced (Supplemental Figure S5E). On the other hand, the mutant of both LIR and FIRs, which was an interaction-deficient mutant for LC3 and FIP200, showed complete abolition of colocalization of CCPG1 with LC3, instead accumulating as large amorphous structures under ER stress conditions. However, no accumulation of CCPG1 was observed when both the luminal domain and ATG protein-interaction motifs were deleted (Supplemental Figure S5E). These data suggest that the localization of CCPG1 to autophagosomes is dependent on LIR and FIRs, but not the luminal domain. In addition, luminal domain-dependent formation of aggregate-like structures by CCPG1 may result from interactions with misfolded proteins in the ER.

## P3H4 is an endogenous substrate for CCPG1-dependent ER-phagy

To identify endogenous substrates for CCPG1-dependent ER-phagy, we searched for proteins that interacted with CCPG1 in a luminal domain-dependent manner. We performed IP using FLAG-CCPG1 and its mutants, as described below, and subjected the immunoprecipitates to mass spectrometry (MS) analysis. MS screening 1 used FLAG-CCPG1 full-length and FLAG-CCPG1 luminal domain deletion as a negative control, and MS screening 2 used FLAG-CCPG1 cytosolic domain deletion (Figure 4A). The resultant immunoprecipitants were analyzed through liquid chromatography with tandem mass spectrometry (LC-MS/MS; Figure 4B). We identified numerous ER luminal proteins, including ER chaperones, ERAD components, glycosidases, and enzymes for collagen maturation. Among these proteins, we focused on P3H4, which was identified in both MS screens and has not yet been studied in the context of autophagy. P3H4 is an ER-resident protein belonging to the Leprecan (leucine proline-enriched proteoglycans) family (Ochs *et al.*, 1996; Gruenwald *et al.*, 2014) and forms a complex with prolyl 3-hydroxylase to regulate lysine hydroxylation of collagen (Heard *et al.*, 2016). P3H4 exhibited CCPG1-luminal domain-dependent interaction with CCPG1 (Figure 4C). To monitor pulse-chased lysosomal degradation of P3H4, we employed a HaloTag-based cleavage assay for P3H4

---

experiments. Differences were statistically analyzed by Dunnett's multiple comparison test. (D–F) Lysosomal degradation of 6xIAPP-RG occurs in a manner dependent on the ER-luminal region of CCPG1. WT and CCPG1-KO HeLa cells expressing 6xIAPP-RG, with or without exogenous HA-CCPG1 (full-length or luminal deletion mutant), were incubated in medium containing Dox and then subjected to flow cytometry, immunofluorescence (IF), and immunoblotting. After 24 h of incubation in Dox-containing medium, the cells were incubated with Dox-free medium for a further 24 h. The fluorescence ratio was calculated for RFP-positive cells. Data represent the mean  $\pm$  SE of three independent experiments. Differences were analyzed using one-way ANOVA and Sidak's multiple comparison test, D. Cells treated with Dox as described were fixed and stained with antibodies against HA-tag and then analyzed using immunofluorescence microscopy. GFP-negative and RFP-positive signals (arrowhead) are indicated. Scale bars represent 10 and 1  $\mu$ m (inset), E. Lysates of each treatment were analyzed through immunoblotting using antibodies against RFP, HA, and  $\beta$ -actin (loading control). # indicates degradative products of IAPP-RG, F. (G) The cells treated with Dox as described above were analyzed through immunoblotting. The band intensities of cleaved RFP and 6xIAPP-RG were quantified, and the ratio of cleaved RFP to 6xIAPP-RG (normalized to the WT) is shown. Data represent the mean  $\pm$  SE of three independent experiments. Differences were analyzed using one-way ANOVA and Sidak's multiple comparison test.



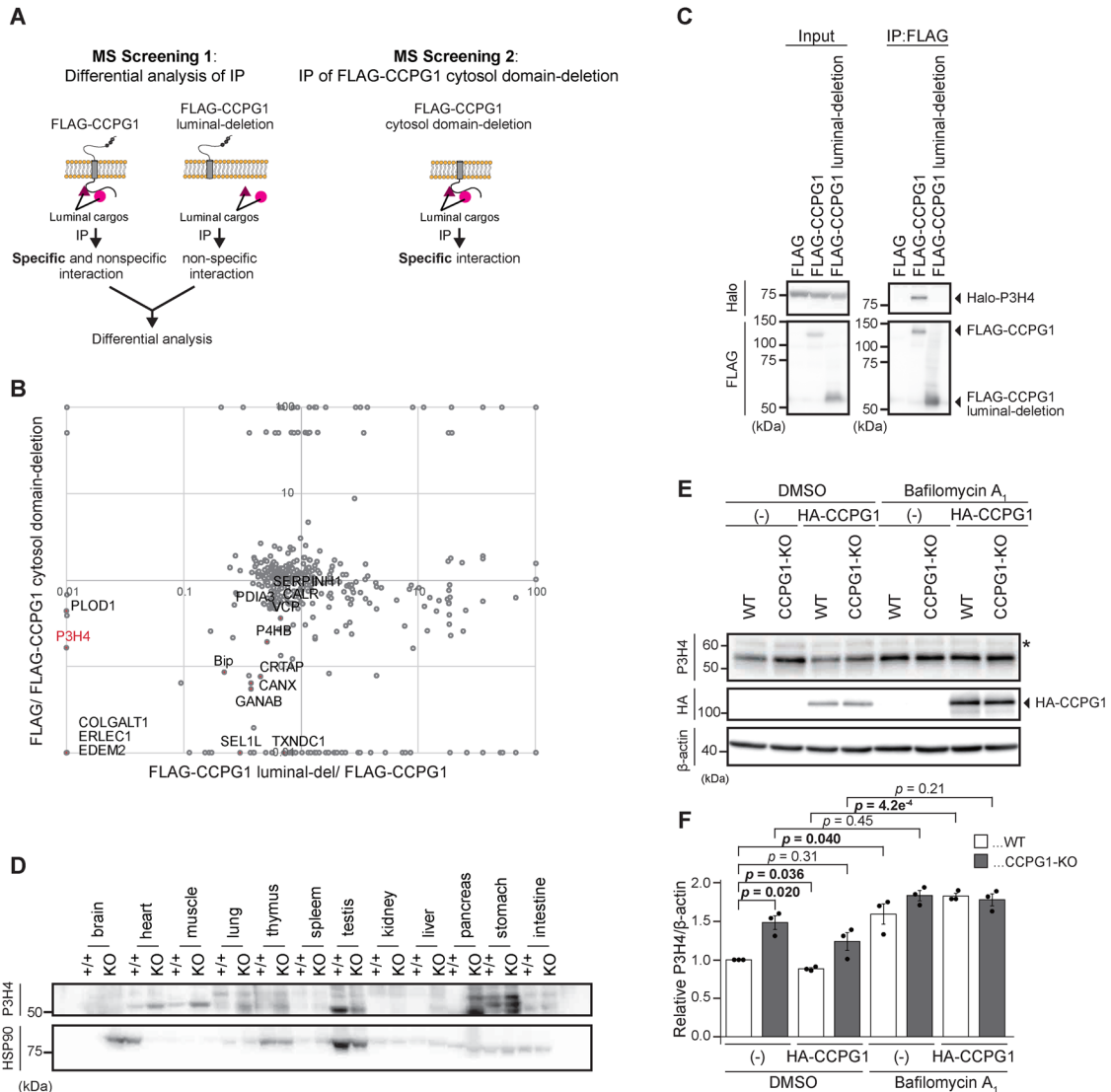


**FIGURE 4:** P3H4 is an endogenous for CCPG1-dependent ER-phagy. (A) Strategy used to identify endogenous CCPG1 luminal domain-interacting proteins. (B) Results of differential interactome screening. Two independent IP and MS analyses were conducted for each LC-MS/MS sample. (C) HEK293T cells transiently expressing ssHalo-P3H4 and WT, or mutated FLAG-CCPG1, were subjected to IP with anti-FLAG antibody and detection with anti-Halo and anti-FLAG antibodies. (D) Immunoblotting of endogenous P3H4 in postnuclear supernatants of the indicated organs from Atg5<sup>+/+</sup>;NSE-Atg5<sup>+/+</sup> and Atg5<sup>-/-</sup>;NSE-Atg5<sup>KO</sup> mice. (E, F) P3H4 accumulated in CCPG1-KO cells. WT or CCPG1-KO cells with or without exogenous HA-CCPG1 were treated with DMSO or bafilomycin A<sub>1</sub> for 24 h and then lysed with lysis buffer. Each cell lysate was analyzed through immunoblotting using antibodies against P3H4, HA-tag, or β-actin (loading control). \* indicates nonspecific band, E. Band intensities were quantified and the ratio of P3H4 to β-actin (normalized to the WT) is shown. Data represent the mean ± SE. Differences were analyzed using one-way ANOVA and Sidak's multiple comparison test, F.

(HaloTag becomes resistant to lysosomal degradation after ligand binding; Yim *et al.*, 2022). HeLa cells stably expressing ssHalo-P3H4 were transfected with siRNA against CCPG1. After 3 d, the cells were exposed to tetramethylrhodamine-conjugated ligand for 1 h and then incubated for 24 h. Generation of the Halo cleavage band was significantly impaired in CCPG1-depleted cells (Supplemental Figure S4, A and B). Cleavage of reporters was restored through reexpression of CCPG1, but not the luminal-domain deletion mutant or LIR/FIR mutants (Supplemental Figure S6, A and B). These data suggest that P3H4 is degraded by CCPG1 in a luminal domain- and autophagy-dependent manner. Notably,

endogenous P3H4 accumulated markedly in the pancreas, stomach, heart, and muscle of adult brain-rescued ATG5-KO mice (Yoshii *et al.*, 2016; Figure 4D), suggesting that some tissues constitutively degrade P3H4 via ER-phagy. Considering that CCPG1 is also highly expressed in exocrine tissues such as the pancreas and stomach (Chino *et al.*, 2019), these results suggest that CCPG1 has a functional relationship with P3H4. P3H4 also accumulated in CCPG1-KO or bafilomycin A<sub>1</sub>-treated HeLa cells (Figure 4, E and F). Additionally, overexpression of HA-CCPG1 reduced the amount of P3H4. These data indicate that P3H4 is an endogenous substrate for CCPG1-dependent ER-phagy.

## Highly conserved ER-luminal regions of CCPG1 contain functional domains

As the ER-luminal region of CCPG1 is essential for ER-phagy-mediated degradation of 6xIAPP and P3H4, we apportioned the luminal region into conserved regions through sequence alignment among vertebrates. Although the length of the CCPG1 sequence varied among species by up to 120 aa, the ER luminal region of CCPG1 contained four highly conserved regions (region A: aa 288–401, region B: aa 411–457, region C: aa 482–550, region D: aa 621–734; Supplemental Figure S7A). We presumed that regions A–D of CCPG1 include the cargo-interacting region (CIR) and generate C-terminal-truncated mutants ( $\Delta 742$ –757,  $\Delta 621$ –757,  $\Delta 551$ –757,  $\Delta 411$ –757, and  $\Delta 289$ –757; Figure 5A). First, we measured bulk ER-phagy activity using ssRFP-GFP-KDEL, an ER-luminal fluorescence reporter for ER-phagy (Chino *et al.*, 2019), and found that overexpression of the full-length sequence or any truncated mutant in CCPG1-KO cells promoted lysosomal degradation of ssRFP-GFP-KDEL (Supplemental Figure S7, B and C), suggesting that the cytosolic region (containing LIR and FIRs) and transmembrane domain of CCPG1 are sufficient for the induction of bulk ER-phagy. The cleavage of ssRFP-GFP-KDEL by some truncated mutants, including  $\Delta 551$ –757 and  $\Delta 411$ –757, compared with full-length CCPG1 was more efficient, probably due to the high expression level. From these results, enhancement of bulk-ER-phagy activity caused by overexpression of the CCPG1 luminal-deletion mutant might result in partial recovery of lysosomal degradation of 6xIAPP (Figure 3E). In contrast, lysosomal degradation of 6xIAPP-RG was not rescued through overexpression of the  $\Delta 411$ –757 and  $\Delta 289$ –757 mutants of CCPG1 in CCPG1-KO cells (Figure 5, B–D), indicating that highly conserved regions within 411–551 aa, including regions B and C, might recognize 6xIAPP for degradation via ER-phagy. We defined the highly conserved regions B–D as CIR 1–3 (Figure 5E).

To characterize these CIRs, we generated CIR1-, CIR2-, and dual CIR1- and CIR2-truncated mutants and analyzed the associated lysosomal degradation of 6xIAPP-RG. Contrary to our expectations, lysosomal degradation of 6xIAPP-RG was rescued by all CIR1- and CIR2-related mutants (Figure 5, F–H). Therefore, we hypothesized that region D, defined as CIR3, may contribute to 6xIAPP degradation along with CIR1, CIR2, or both. We found that truncated CCPG1 with both CIR1 and CIR3 deleted was unable to restore the lysosomal degradation of 6xIAPP-RG (Figure 5, G and H). Alternatively, bulk ER-phagy detected using ssRFP-GFP-KDEL was restored with overexpression of any CIR-related mutants of CCPG1 (Supplemental Figure S7, C and D). These results demonstrate that the ER luminal region of CCPG1 contains functional domains, that is, CIRs, required for the selective degradation of 6xIAPP.

We conducted similar experiments using another cargo, P3H4. CCPG1 mutants lacking CIR2 did not rescue the lysosomal degradation of RG-P3H4 (Figure 5, I and J). Furthermore, CCPG1 $\Delta$ CIR2 no longer colocalized to the dot-like structures observed for RG-P3H4, in contrast to the full-length sequence and other mutants of CCPG1 (Figure 5K). These findings suggest that P3H4 undergoes CIR2-dependent ER-phagy degradation and that CCPG1 contains multiple cargo recognition sequences in the ER luminal region.

### CIR1 interacts directly with IAPP, while CIR2 interacts with P3H4

Next, we verified whether CCPG1 interacts directly with P3H4 and 6xIAPP. All recombinant proteins containing the full length of the ER luminal region, each CIR region alone (CIRs 1–3), CIR1+3 of CCPG1, P3H4, and 6xIAPP combined with small tags (ALFA, HA, and FLAG; Götzke *et al.*, 2019), and dihydrofolate reductase (DHFR) for stabiliza-

tion (Iwakura *et al.*, 1992) were synthesized in vitro using a cell-free protein synthesis system (Shimizu *et al.*, 2001, 2005). Expression levels were estimated through immunoblotting, and the synthesized proteins were mixed at a 1:3 volume ratio (antigen:binding partner) in lysis buffer for IP using specific antibodies. 6xIAPP interacted efficiently with the entire C-terminal region (241–757) of CCPG1 (Figure 6, A and B). Although HA-6xIAPP did not coprecipitate with CIR2 and CIR3 alone, it did coprecipitate with CIR1 alone, and with CIR1+CIR3. In contrast, the entire C-terminal region and CIR2 alone coimmunoprecipitated by HA-P3H4 (Figure 6, C and D). These observations suggest that the CIRs of CCPG1 directly interact with ER luminal cargos, and that different CIRs contribute to the recognition of different cargos.

### The ER luminal region of CCPG1 simultaneously recognizes multiple cargos

As 6xIAPP and P3H4 interacted directly with different CIRs of CCPG1, we hypothesized that a single molecule of CCPG1 could interact simultaneously with 6xIAPP and P3H4. Therefore, we checked for competitive inhibition using excess levels of the same recombinant proteins with different tags synthesized using a cell-free protein translation system. The presence of excess FLAG-P3H4 inhibited co-IP of HA-P3H4 with ALFA-CCPG1 (full-length of C-terminal; Figure 7, A and B), while the addition of excess DHFR-FLAG had no effect on that interaction. Similarly, co-IP of HA-6xIAPP by ALFA-CCPG1 was inhibited by excess FLAG-6xIAPP (Figure 7, C and D), indicating that interaction of the cargo with CCPG1 can compete with the same excess cargos under in vitro conditions.

Then we confirmed competitive inhibition of 6xIAPP and P3H4 against CCPG1. Recombinant ALFA-CCPG1 was mixed with HA-P3H4 or FLAG-6xIAPP or both, and then immunoprecipitated using anti-ALFA antibody beads. The presence of P3H4 had no inhibitory effect on binding between 6xIAPP and CCPG1; similarly, 6xIAPP did not inhibit the binding of CCPG1 to P3H4 (Figure 7, E and F). This result suggests that a single CCPG1 molecule interacts simultaneously with multiple cargos.

## DISCUSSION

In this study, we found that CCPG1 directly interacts with ER luminal proteins via CIRs, which recognize different types of cargo (Figure 7G). CCPG1 is a receptor not only for LC3 and FIP200, but also for ER luminal proteins (via its long ER luminal region). Therefore, our findings provide new insights, indicating that CCPG1 is a bispecific receptor for ER luminal cargos and the autophagic membrane; it drives selective ER-phagy and the cargo selectivity thereof, thereby promoting efficient degradation of particular cargos through ER-phagy.

6xIAPP promotes primary nucleation and increases proteotoxicity (Kayatekin *et al.*, 2018). Excessive expression of 6xIAPP in yeast clogs the translocon, which is then removed through proteasomal degradation via Ste24. Upon ZMPSTE24 inhibition by Lopinavir, 6xIAPP proteotoxicity also decreases cell viability in mammalian pancreatic cells (Kayatekin *et al.*, 2018). We employed 6xIAPP fused with several different tags (fluorescent proteins or HA-tags) and the KDEL signal as a model ER-phagy substrate. Moreover, we found that 6xIAPP is primarily translocated within the ER at a steady state in mammalian cells, as verified by the analysis of N-glycosylation using a construct fused with the glycosylation site from opsin (Supplemental Figure S1D). Aggregated 6xIAPP was primarily degraded through autophagy under the investigated conditions (Figure 2). On the other hand, proteasome inhibition led to the accumulation of 6xIAPP, which was detected in the insoluble fraction without

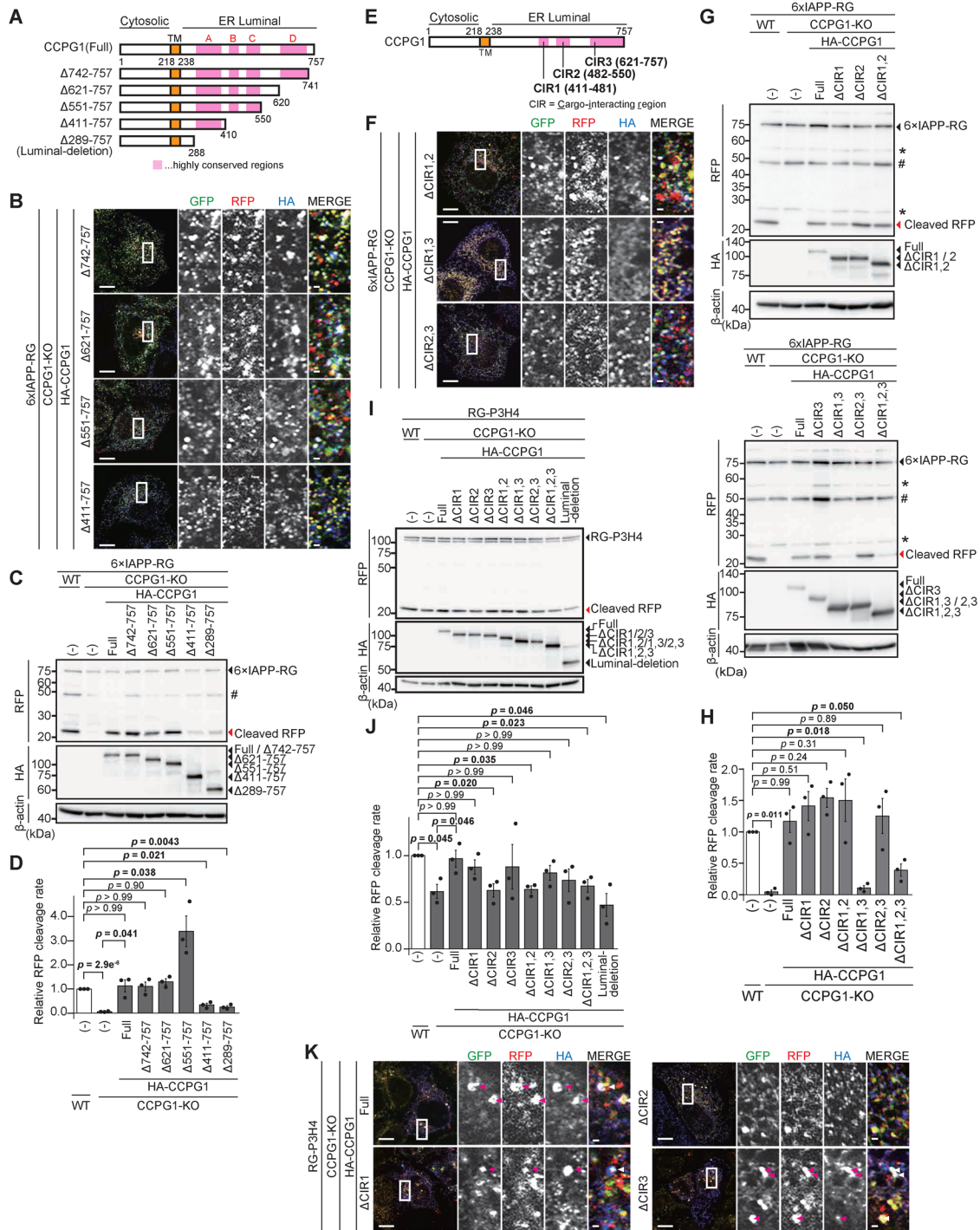


**FIGURE 5:** The highly conserved C-terminal region of CCPG1 contains functional domains. (A) Diagram of the truncated mutants of CCPG1. (B–D) The ER luminal region of CCPG1 at 411–757 aa is required for lysosomal degradation of 6xIAPP. CCPG1 KO HeLa cells coexpressing the indicated CCPG1 mutants (constitutive) and 6xIAPP-RG (Tet-On) were incubated with medium containing Dox for 48 h and subjected to IF and immunoblotting. Cells were stained with antibodies against HA-tag and analyzed through immunofluorescence microscopy. Scale bars represent 10 and 1  $\mu$ m (inset). B. Cell lysates were analyzed through immunoblotting with antibodies against RFP, HA-tag, and  $\beta$ -actin (loading control). # indicates degradative products of 6xIAPP-RG, C. The band intensities of cleaved RFP and 6xIAPP-RG were quantified and the ratio of cleaved RFP to 6xIAPP-RG (normalized to the WT) is shown. Data represent the mean  $\pm$  SE of three independent experiments. Differences were analyzed using one-way ANOVA and Sidak's multiple comparison test, D. (E) Diagram of cargo-interacting region (CIR) mutants of CCPG1. (F–H) Both CIR1 and CIR3 of CCPG1 are required for lysosomal degradation of 6xIAPP. Tet-On WT HeLa cells and CCPG1 KO HeLa cells coexpressing the indicated CIR mutants of CCPG1 (stably) and 6xIAPP-RG (Tet-On) were cultured with Dox for 48 h and then subjected to IF and immunoblotting. Cells were stained with antibodies against HA-tag and analyzed through immunofluorescence microscopy. Scale bars represent 10 and 1  $\mu$ m (inset). F. Cell lysates were analyzed through immunoblotting using antibodies against RFP, HA-tag, and  $\beta$ -actin (loading control). # indicates degradative products of 6xIAPP-RG. \* indicates



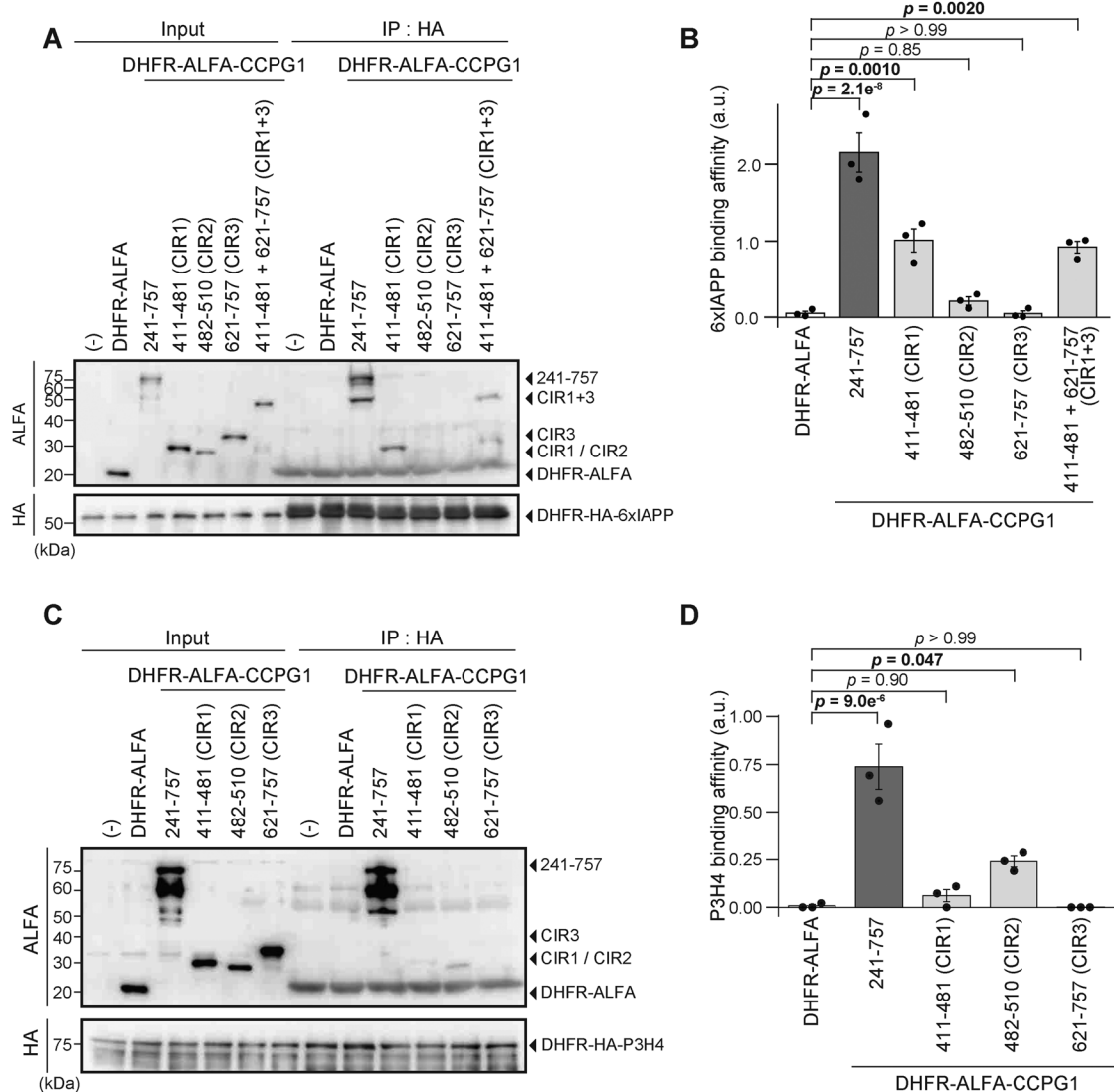


**FIGURE 6:** CIR1 and CIR3 interact directly with 6xIAPP, while CIR2 interacts with P3H4. (A, B) CIR1 of CCPG1 interacts directly with 6xIAPP in vitro. DHFR-ALFA-tagged C-terminal truncated mutants of CCPG1 and DHFR-HA-6xIAPP synthesized using a cell-free protein synthesis system were mixed with anti-HA antibody-conjugated Sepharose and incubated at 4°C for 1 h. After washing, eluates from the Sepharose were analyzed through immunoblotting with antibodies against ALFA-tag and HA-tag, A. The band intensities of DHFR-tag and the luminal domains of CCPG1 were quantified; the ratio of IP to input is shown. Data represent the mean  $\pm$  SE of three independent experiments. Differences were statistically analyzed by Dunnett's multiple comparison test, B. (C, D) CIR2 of CCPG1 interacts directly with P3H4 in vitro. DHFR-ALFA-tagged C-terminal truncated mutants of CCPG1 and DHFR-HA-P3H4 were synthesized using a cell-free protein synthesis system and then mixed with anti-HA antibody-conjugated Sepharose and incubated at 4°C for 1 h. After washing, eluates from the Sepharose were analyzed through immunoblotting with antibodies against ALFA-tag and HA-tag, C. The band intensities of DHFR-tag and luminal domains of CCPG1 were quantified; the ratio of IP to input is shown. Data represent the mean  $\pm$  SE of three independent experiments. Differences were statistically analyzed by Dunnett's multiple comparison test, D.

nonspecific bands, G. Band intensities of cleaved RFP and 6xIAPP-RG were quantified and the ratio of cleaved RFP to 6xIAPP-RG (normalized to the WT) is shown. Data represent the mean  $\pm$  SE of three independent experiments. Differences were statistically analyzed by Dunnett's multiple comparison test, H. (I–K) CIR2 of CCPG1 is required for lysosomal degradation of P3H4. Tet-On WT HeLa cells and CCPG1 KO HeLa cells coexpressing full-length or CIR-mutant CCPG1 (constitutive) and ssRFP-GFP-P3H4 (RG-P3H4) (Tet-On) were cultured with Dox for 48 h and then subjected to IF and immunoblotting. Cell lysates were analyzed through immunoblotting using antibodies against RFP, HA-tag, and  $\beta$ -actin (loading control), I. The band intensities of cleaved RFP and RG-P3H4 were quantified, and the ratio of cleaved RFP to RG-P3H4 (normalized to the WT) is shown. Data represent the mean  $\pm$  SE of three independent experiments. Differences were analyzed using one-way ANOVA and Sidak's multiple comparison test, J. Cells were stained with antibodies against HA-tag and analyzed through immunofluorescence microscopy. GFP and RFP-positive signals colocalizing with HA-positive structures (arrowhead) are indicated. Scale bars represent 10 and 1  $\mu$ m (inset), K.

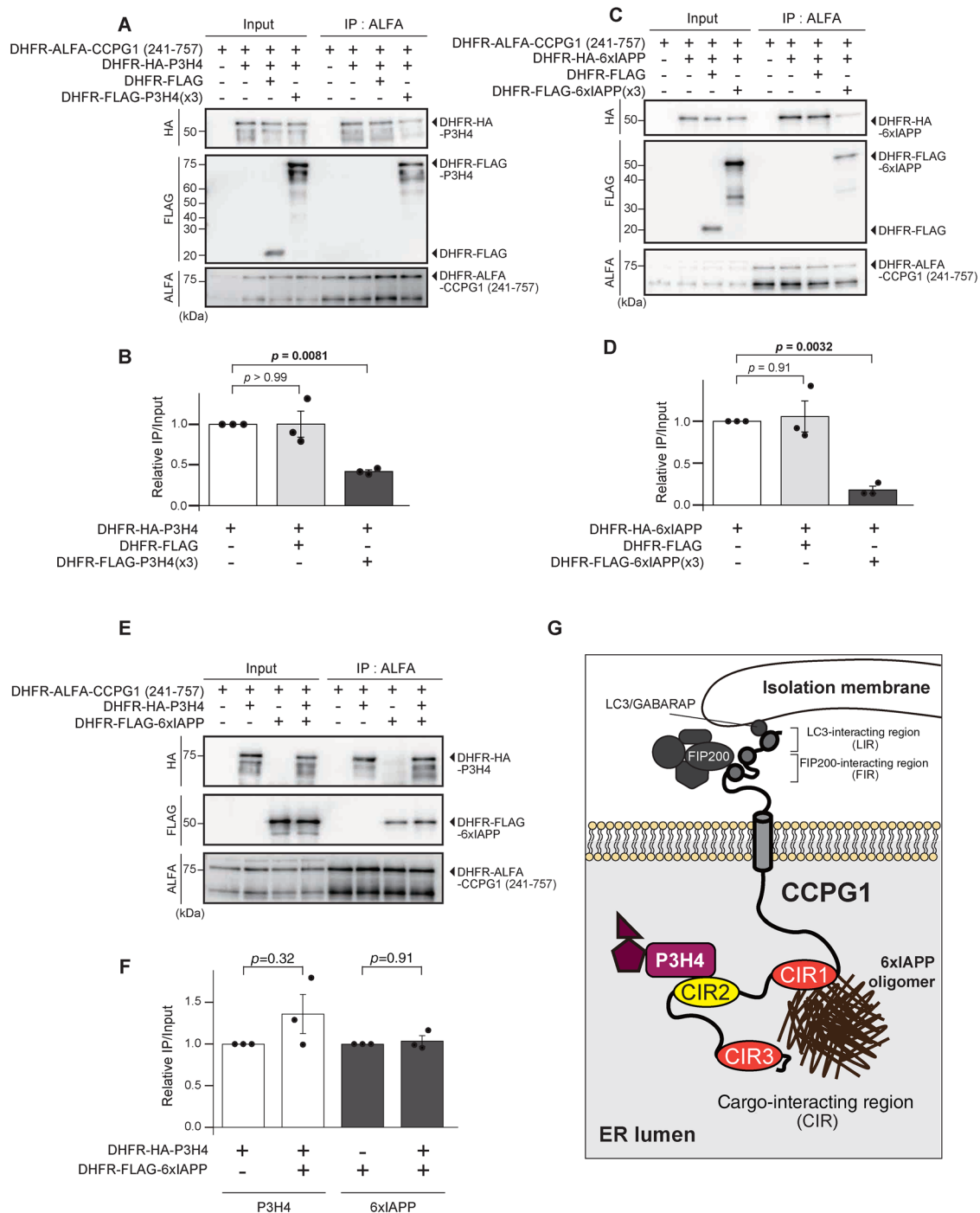


**FIGURE 7:** The ER luminal region of CCPG1 simultaneously recognizes multiple cargos. (A–D) The same ER luminal cargo competitively inhibits the interaction with CCPG1. DHFR-ALFA-CCPG1 (C-terminal full-length) and DHFR-HA-P3H4 (or 6xIAPP) with or without DHFR-FLAG-P3H4 (or 6xIAPP) or DHFR-FLAG were synthesized using a cell-free protein synthesis system, mixed with anti-ALFA Sepharose, and then incubated at 4°C for 1 h. FLAG-tagged products were added at three times the level of HA-tagged cargos (indicated as × 3). Eluted products were analyzed through immunoblotting with antibodies against ALFA-, FLAG-, and HA-tag, A and C. The bar graph shows the ratio between the indicated band intensities. Data represent the mean ± SE of three independent experiments. Differences were statistically analyzed by Dunnett’s multiple comparison test (B and D). (E, F) Different ER luminal cargos are able to interact with CCPG1 simultaneously. Synthesized DHFR-HA-P3H4 and DHFR-FLAG-6xIAPP were mixed with DHFR-ALFA-CCPG1 (C-terminal), either alone or in combination. Anti-ALFA beads were added to the mixture, which was allowed to react at 4°C for 1 h. After washing four times with 1 × lysis buffer, SDS sample buffer was added and each eluate was analyzed through immunoblotting using antibodies against ALFA-, FLAG-, and HA-tag, E. The bar graph shows the ratio of IP to input ( $n = 3$ ). The data represent mean ± SE. Differences were statistically analyzed by Student’s *t* test, F. (G) A simultaneous recognition model, in which CCPG1 interacts directly with multiple ER luminal cargos.

glycosylation (Supplemental Figure S2H); this indicated that 6xlAPP was mislocalized to the cytoplasm because of stress-induced inhibition of protein translocation (Kang *et al.*, 2006) or was dislocated from the clogged ER translocon by ZMPSTE24, a mammalian homologue of yeast Ste24 (Ast *et al.*, 2016; Kayatekin *et al.*, 2018). These results demonstrate that 6xlAPP in mammals does not always clog the translocon, but some proportion may be successfully translocated into the ER, where aggregated 6xlAPP is targeted for ER-phagy. Analysis of cells expressing low and high levels of 6xlAPP indicated a difference in dependence (Supplemental Figure S2, F and G). Low expression levels of 6xlAPP were mainly degraded through a nonlysosomal pathway. On the other hand, highly expressed 6xlAPP was largely degraded through the lysosomal pathway (Supplemental Figure S2, F and G). We speculated that 6xlAPP aggregated in the ER is an ERAD-inefficient substrate, similar to aggregated procollagen (Ishida *et al.*, 2009). 6xlAPP formed large oligomers under our conditions (Supplemental Figure S1, A and B). The conformation of aggregated 6xlAPP at high concentrations in the ER might lead to its recognition by CCPG1.

We observed that the overexpression of 6xlAPP alone is sufficient to induce autophagy (Figure 2B; Supplemental Figure S3, B-F), likely because the increased abundance of CCPG1 is directly recognized by both FIP200 and LC3 (Figure 3A; Supplemental Figure S4, A and B). This finding is supported by a previous report that overexpression of WT CCPG1, but not mutant LIR or FIR, promotes ER-phagy (Smith *et al.*, 2018). This raises the question of how 6xlAPP induces CCPG1 expression. ER stress induces CCPG1 expression (Smith *et al.*, 2018). Moreover, the UPR factors PERK, XBP1, and MIST1 are associated with CCPG1 transcription (Tian *et al.*, 2010; Adamson *et al.*, 2016). However, we did not detect activation of the UPR pathway by 6xlAPP overexpression in HeLa cells, although ER-phagy was induced (unpublished data). Future work is needed to identify the specific transcription factor(s) responsible for CCPG1 induction by 6xlAPP. Another open question is how CCPG1 induces autophagy. We initially assumed that a luminal cargo transduces a signal from the ER lumen to the cytoplasmic side to induce ER-phagy, similarly to the induction of the UPR; if this is the case, cargo binding to CCPG1 might trigger ER-phagy. However, overexpression of a CCPG1 mutant lacking the whole ER luminal region induced autophagy (Supplemental Figure S7, B and C). Therefore, the expression of CCPG1, which recruits FIP200 and LC3 to the ER membrane, might be sufficient to initiate ER-phagy, even without an ER luminal cargo. Although this mechanism may not be elegant, it is very straightforward, and CCPG1-dependent ER-phagy does not require any additional signal transduction pathways.

As CCPG1 has the largest ER luminal domain among known ER-phagy receptors, it has been speculated that CCPG1 recognizes ER luminal proteins (Smith and Wilkinson, 2017; Grumati *et al.*, 2018; Smith *et al.*, 2018; Wilkinson, 2020). We revealed that CCPG1 interacts directly with cargos, including 6xlAPP and P3H4. P3H4 was reported to play a role in catalyzing the complex hydroxylation process of collagen chains. Physiologically, P3H4 is a prognostic factor for lung adenocarcinoma and bladder cancer (Li *et al.*, 2018; Jin *et al.*, 2021); it contributes to cancer invasion and growth (Hao *et al.*, 2020), suggesting that CCPG1 may have a protective effect against these cancers. In addition, endogenous P3H4 accumulated in the pancreas and stomach of autophagy-deficient mice (Figure 4D), suggested that it undergoes degradation dependent on the autophagy-lysosome pathway, particularly in exocrine organs.

Several ER chaperones, including BiP, calnexin, PDIA1, PDIA3, CALR, and TXNDC5, were identified by our MS analysis of proteins binding to the luminal region of CCPG1 (Figure 4, A and B). This is

consistent with a previous finding that ER chaperones, including PDIA6, accumulated in the pancreas of CCPG1 hypomorphic mice (Smith *et al.*, 2018). As FAM134B has been reported to bind to BiP and calnexin, which mediates the capture of luminal misfolded proteins under ER stress conditions (Fregno *et al.*, 2018; Forrester *et al.*, 2019; Chipurupalli *et al.*, 2022), CCPG1 may employ a similar mechanism, in which ER chaperones mediate the degradation of luminal proteins through ER-phagy. CCPG1 is an ER stress-responsive gene, suggesting that ER-phagy may share common substrates with ERAD, and that cross-talk may exist, depending on the amount of degradation. In this scenario, although ER-phagy exhibits more extensive selective recognition of unfolded proteins, its substrate selectivity might be similar to the UPR, such that direct recognition of a substrate by the luminal region of CCPG1 may contribute to ER-phagy-specific selectivity.

Homology searches were performed with the Position-Specific Iterative Basic Local Alignment Search Tool (PSI-BLAST) using human sequences of CIRs from CCPG1; however, we detected no proteins containing similar domains. Moreover, further searches using the InterPro database (v90.0; Blum *et al.*, 2021) identified no paralog or proteins with conserved CIR-related regions. In addition, no similarity among CIRs in CCPG1 was found through sequence alignment. The AlphaFold tool predicted that CIRs 1–3 have different structures (Jumper *et al.*, 2021; Varadi *et al.*, 2022), and our data indicated different cargo selectivity among these CIRs; this indicated that each CIR recognizes the cargo using different machinery. Therefore, we speculated that the ER luminal region of CCPG1 has unique features related to the recognition of ER-phagy substrates. Future work is needed to identify the specific motifs that bind ER-phagy substrates and reveal the detailed mechanisms of substrate selectivity.

## MATERIALS AND METHODS

[Request a protocol](#) through *Bio-protocol*.

### Antibodies

Rabbit polyclonal anti-LAMP1 antibodies were a gift from Y. Tanaka (Kyusyu University). Rabbit polyclonal anti-TRAP $\alpha$  antibodies were a gift from R.S. Hegde (MRC LMB). Mouse monoclonal anti-HA (clone 16B12, 901502) was purchased from BioLegend Funakoshi (Tokyo, Japan). Mouse monoclonal anti-RFP (M204-3) and anti-LC3 (M152-3) antibodies and rabbit polyclonal anti-LC3 (PM036), anti-p62 (PM045), and anti-ATG9A (PD042MS) antibodies were purchased from MBL (Tokyo, Japan). Mouse monoclonal anti- $\beta$ -actin (281-98721), anti-GFP (clone mFX75, 012-22541), and anti-FLAG (018-22381) antibodies were purchased from Wako (Osaka, Japan). Mouse monoclonal anti-RPL19 (WH0006143M1), anti- $\beta$ -actin (A2228), and anti-FLAG (F4042) antibodies were purchased from Sigma-Aldrich (St. Louis, MO, USA). Mouse monoclonal anti-HSP90 (610419) antibodies were purchased from BD Biosciences (Tokyo, Japan). Mouse monoclonal anti-Halo (G9211) antibody was purchased from Promega (Madison, WI). Rabbit polyclonal anti-FAM134B (21537-1-AP), anti-RTN3 (12055-2-AP), anti-CCPG1 (13861-1-AP), anti-TEX264 (25858-1-AP), anti-RB1CC1 (FIP200) (17250-1-AP), anti-ATG5 (10181-2-AP), and anti-Histone-H3 (17168-1-AP) antibodies were purchased from Proteintech (Tokyo, Japan). Rabbit polyclonal anti-SEC62 (NBP1-84045) antibodies were purchased from Novus Biologicals (Centennial, CO). Rabbit polyclonal anti-P3H4 (A13754) antibodies were purchased from ABclonal (Woburn, MA). Rabbit polyclonal anti-ALFA antibodies were raised in rabbits through immunization with the ALFA peptide (Eurofins). GFP-nanobody and ALFA tag-nanobody Sepharose were generated



through conjugation of GFP-nanobody protein purified from pOP-INE GFP nanobody (plasmid 49172; Addgene, Watertown, MA) and ALFA tag-nanobody protein (Götzke *et al.*, 2019) purified from pR-SET-A ALFA-His to N-hydroxy succinimide-activated Sepharose 4 Fast Flow (GE Healthcare, Chicago, IL). Mouse monoclonal anti-FLAG M2 affinity gel (A2220) and anti-FLAG M2 magnetic beads (M8823) were purchased from Sigma-Aldrich. Mouse monoclonal anti-HA conjugated Sepharose (014-23081) was purchased from Wako.

### Plasmids

To generate pCW\_1x (or 6x) IAPP-RFP-GFP-KDEL or 1x (or 6x) IAPP-RFP-GFP, IAPP-related constructs, human IAPP and 6xIAPP sequences (synthesized using gBlocks Gene Fragments; Integrated DNA Technologies; Coralville, IA) were inserted into the pCW57.1 vector (plasmid #41393; Addgene) along with DNA encoding the mCherry, super-folder GFP (sfGFP), and, if indicated, KDEL sequences. For pCW\_1x (or 6x) IAPP-HA-KDEL, each IAPP sequence and 3 × hemagglutinin (HA)-tag was used. pCW\_1x (or 6x) IAPP-Gly-HA-KDEL was generated through insertion of the N-glycosylation site from opsin (Pedrazzini *et al.*, 2000) into pCW\_1x (or 6x) IAPP-HA-KDEL. To generate pCW ssRFP-GFP-KDEL, the signal sequence of prolactin and the mCherry, super-folder GFP, and KDEL sequences were subcloned into the pCW57.1 vector. For pCW ssRFP-GFP-P3H4, cDNA of human P3H4 amplified from total cDNA of HEK293T cells was used. To generate full-length or truncated CCPG1 constructs, cDNA of CCPG1s was amplified from HEK293FT total cDNA and inserted into the pLenti cytomegalovirus vector GFP Puro (plasmid 17448; Addgene) or pMRX-IB (Morita *et al.*, 2018); these plasmids were generated from pMXs (Kitamura *et al.*, 2003) along with enhanced GFP, 3xFLAG-tag, or 3xHA-tag. Truncated constructs were prepared through PCR-mediated site-directed mutagenesis. To generate pMRXIB\_RFP-GFP-LC3 and pMRXIB\_RFP-GFP-Cytb5, cDNA of rat LC3 and the transmembrane domain of Cytb5 were amplified from pMXs-IP-EGFP-LC3 (plasmid 38195; Addgene) and pMXs-puro GFP-b5 ER (plasmid 38274; Addgene) and inserted into the pMRX-IB vector. For the ATG- or ER-phagy receptor gene-targeted CRISPR vector, the specific sgRNA sequences were inserted into lentiCRISPR v2 hygro (plasmid 98291; Addgene) or lentiGuide-puro (plasmid 52963; Addgene). For plasmids with a cell-free protein synthesis system *in vitro*, DHFR (amplified from PURExpress DHFR), 3xHA-tag, 3xFLAG-tag, ALFA-tag, P3H4, and the indicated regions of CCPG1 (amplified from total cDNA of HEK293FT) were inserted into a PUR-Express plasmid (provided with the PURE system kit from New England Biolabs, Ipswich, MA). pCMV-VSVG (plasmid 8454; Addgene) and psPAX2 (plasmid 12260; Addgene) were used for lentivirus production. pCMV-VSVG and Gag were used for retrovirus production.

### Cell culture

HeLa and HEK293FT cells were cultured in DMEM (Nacalai Tesque, Kyoto, Japan) supplemented with 10% fetal bovine serum (FBS; MP Biomedicals, Santa Ana, CA) and 50 mg/ml penicillin and streptomycin (regular medium) in a 5% CO<sub>2</sub> incubator. Tetracycline-On (Tet-On) cells were generated through lentiviral transduction with a pCW57.1 vector containing the single-vector Tet-On component.

For compound treatment, cells were incubated at the indicated times with 0.2 μM bafilomycin A<sub>1</sub> (LC Laboratories, Woburn, MA), 1 μM Torin 1 (Tocris Bioscience, Ellisville, MO), 2 μg/ml tunicamycin (Sigma-Aldrich), 0.2 μM thapsigargin (Santa Cruz Biotechnology, Dallas, TX), 10 μg/ml E64d (Peptide Institute, Osaka, Japan), 100 μM pepstatin A (Peptide Institute), 20 μg/ml leupeptin (Peptide Institute), or 1 μg/ml Dox (Clontech, Mountain View, CA).

### Generation of a KO cell line using CRISPR/Cas9 gene editing (mixed population of WT and KO cells)

SgRNA sequences for KO cells were designed using CHOPCHOP [FIP200 (5'-GGCTGCAATCATGGCCAACC-3'): Atg5 (5'-AAG-AGTAAGTTATTTGACGT-3'): Atg9A (5'-AGGATATTCGAGAGAA-GAAG-3'): CCPG1(5'-ACAGTGATTCATCTTGTGGT-3'): FAM134B (5'-ACTCTTTGGCAGCAACCGTG-3'): RTN3 (5'-AAGAAGA-CTGGGTTTGTCTT-3'): SEC62 (5'-CCACCAATATGATGGGT-CAC-3'): TEX264 (5'-GCTACTACTGGCCTGATTG-3')] and cloned into lentiCRISPR v2 hygro (plasmid 98291; Addgene) or lentiGuide-puro (plasmid 52963; Addgene). HeLa cells were infected with the lentivirus and then cultured for 7 d under hygromycin/puromycin selection. The hygromycin/puromycin-resistant cells were used as KO cell lines.

### Generation of a clonal KO cell line using CRISPR/Cas9 gene editing

To generate clonal HeLa CCPG1 KO cells, HeLa cells were transfected with pSpCas9(BB)-2A-Puro (PX459) V2.0 (plasmid 62988; Addgene) containing the sgRNA sequence of CCPG1. Puromycin was transiently applied for 24 h posttransfection. After culturing for >5 d, single cell clones were isolated through dilution into 96-well plates and screened for successful KO of CCPG1 through immunoblotting.

### Generation of stable cell lines through lentiviral and retroviral infection

Stable cell lines were generated using lentiviral and retroviral expression systems. HEK293FT cells were transiently cotransfected with lentiviral or retroviral vectors using PEI MAX reagent (Polysciences, Warrington, PA). After culturing for 72 h, the growth medium containing the virus was centrifuged, and the resulting supernatant was collected. HeLa cells were incubated with this virus-containing medium for 48 h and then selected with 1 μg/ml puromycin (InvivoGen, San Diego, CA), 5 μg/ml blasticidin S (Wako), 100 μg/ml hygromycin B (Wako), or 500 μg/ml G418 (Nacalai Tesque).

### Immunoblotting

Cells were washed with cold phosphate-buffered saline (PBS) and lysed in lysis buffer (1% Triton X-100, 50 mM Tris-HCl pH 7.5, 1 mM EDTA [EDTA], and 150 mM NaCl) supplemented with protease inhibitor cocktail (EDTA-free; Nacalai Tesque) and 1 mM phenylmethanesulfonyl fluoride for the collection of soluble fractions, or 1xSDS sample buffer (0.0625 mM Tris-HCl pH 6.8, 2% SDS, 10% 2-mercaptoethanol, and 10% glycerol) for the collection of whole-cell lysates, for 15 min at 4°C. The soluble lysates were clarified through centrifugation at 20,630 × *g* for 5 min, and 6 × sodium dodecyl sulfate (SDS) sample buffer was added. The samples were heated to 95°C for 5 min before SDS/polyacrylamide gel electrophoresis (SDS/PAGE), in which 20 μg of protein per lane was separated and then transferred to a polyvinylidene disulfide membrane (Millipore, Burlington, MA). Immunoblot analysis was performed with the indicated antibodies suspended in Signal Enhancer Hikari (Nacalai Tesque) and the immunoreactive proteins were visualized using ImmunoStar Zeta (Wako).

### siRNA knockdown experiments

Stealth RNAi oligonucleotides were purchased from Thermo Fisher Scientific (Waltham, MA). The following sequences were used: si-CCPG1, 5'-UCCAAUAGAUACUGUCUUCGGG -3' and siLuciferase (siLuc), 5'-AAUUAAGUCCGUUCUAAGGUUCC-3'. The stealth RNAi oligonucleotides were transfected into cells using

Lipofectamine RNAiMAX (13778150; Thermo Fisher Scientific) according to the manufacturer's instructions.

## Mice

All animal experiments were approved by the Institutional Animal Care and Use Committee of the University of Tokyo. *Atg5<sup>-/-</sup>*; *NSE-Atg5* mice (Yoshii *et al.*, 2016) and *Fip200<sup>flox/flox</sup>*; *Nestin-Cre* mice (Liang *et al.*, 2010) have been described previously. To obtain postnuclear supernatants, tissue homogenates were centrifuged at 500 × *g* for 10 min and the supernatants were boiled in sample buffer.

## LC-MS/MS analysis of FLAG-CCPG1 immunoprecipitates

HeLa stably expressing FLAG-CCPG1, as well as the FLAG-CCPG1 luminal-deletion mutant and FLAG and FLAG-CCPG1 cytosol-deletion mutants, were incubated and lysed with lysis buffer (50 mM Tris-HCl, pH 7.5, 150 mM NaCl, 1% NP-40, and complete EDTA-free protease inhibitor [03969-21; Nacalai Tesque]). After centrifugation at 17,700 × *g* for 10 min, the supernatants were incubated with anti-FLAG M2 magnetic beads for 3 h at 4°C with gentle rotation. The eluted proteins were enzymatically digested according to a phase-transfer surfactant (PTS) protocol (Rappsilber *et al.*, 2007). Then 50 µl of each eluted sample was mixed with 85 µl PTS buffer. Samples were reduced with 10 mM dithiothreitol at room temperature for 30 min and alkylated with 50 mM 2-iodoacetamide (804744; Sigma-Aldrich) at room temperature for 30 min. Next, samples were diluted fivefold through addition of 50 mM  $\text{NH}_4\text{HCO}_3$  solution followed by digestion with 1 µg of lysyl endopeptidase (LysC; 121-05063; Wako) at 37°C for 4 h. Samples were further digested with 1 µg trypsin at 37°C for 8 h. An equal volume of ethyl acetate acidified with 0.5% trifluoroacetic acid (TFA) was added to the digested samples. After centrifugation twice at 10,000 × *g* for 10 min at room temperature, the aqueous phase containing the peptides was collected and dried using a SpeedVac concentrator (Thermo Fisher Scientific). The dried peptides were solubilized in 100 µl of 2% acetonitrile and 0.1% TFA, and the peptide mixture was trapped on a handmade C18 STAGE tip prepared as described previously (Boersema *et al.*, 2009). The trapped peptides were subjected to a previously reported dimethyl-labeling procedure (Boersema *et al.*, 2009). Subsequently,  $\text{CH}_2\text{O}$  and  $\text{NaBH}_3\text{CN}$  (light label) were added to the FLAG-only sample. Similarly,  $\text{CD}_2\text{O}$  and  $\text{NaBH}_3\text{CN}$  (heavy label) were added to the FLAG-NEK9 sample. The dimethyl-labeled peptides remaining on the tip were eluted with 100 µl of 80% acetonitrile and 0.1% TFA. The light- and heavy-label eluates were mixed and dried using a SpeedVac concentrator. Each sample was dissolved in 2% acetonitrile and 0.1% TFA and loaded into the LC-MS system with an Orbitrap Exploris 480 MS instrument (Thermo Fisher Scientific) equipped with a nano-high-performance liquid chromatography system (Advance UHPLC; Bruker Daltonics, Billerica, MA, USA) and HTC-Pal autosampler (CTC Analytics, Zwingen, Switzerland) with a trap column (0.3 × 5 mm, L-column ODS; Chemicals Evaluation and Research Institute, Tokyo, Japan). Samples were separated using a gradient of mobile phases A (0.1% [v/v] formic acid in  $\text{H}_2\text{O}$ ) and B (0.1% [v/v] formic acid in acetonitrile) at a flow rate of 300 nL/min (4–32% B for 190 min, 32–95% B for 1 min, 95% B for 2 min, 95% to 4% B for 1 min, and 4% B for 6 min) with a homemade capillary column (length 200 mm and inner diameter 100 µm) packed with 2-µm C18 resin (L-column2; Chemicals Evaluation and Research Institute). Then the eluted peptides were electrosprayed (2.1 kV) and introduced into the MS instrument. Data were obtained in positive ion mode for data-dependent MS/MS (ddMS<sup>2</sup>) acquisition. Full MS spectra were obtained across a scan range of 350–1800 m/z with 60,000 full width at half maximum (FWHM) resolution at 200 m/z.

MS<sup>2</sup> spectra were obtained with 7500 FWHM resolution at 200 m/z. For ddMS<sup>2</sup> acquisition, full MS spectra were obtained every 3 s and MS<sup>2</sup> spectra were obtained during the 3 s intervals. The most abundant precursor ions (excluding isotopes of a cluster) above the  $5.0 \times 10^3$  intensity threshold with a charge state from 2+ to 7+ were selected using a 2.0-*m/z* isolation window. A 20-s dynamic exclusion period was applied. The raw data obtained were used for a database search (UniProt reviewed the mouse database on September 13, 2018) with the Sequest HT algorithm running on the Proteome Discoverer 2.5 platform (Thermo Fisher Scientific). The parameters for database searches were as follows: peptide cleavage was set to trypsin; missed cleavage sites were allowed for up to two residues; peptide lengths were set to 6–144 aa; and mass tolerances were set to 10 ppm for precursor ions and 0.02 Da for fragment ions. Carbamidomethylation of cysteine and dimethylation [H(4)C(2) or D(4)C(2)] of lysin and the peptide N-terminus were set as fixed modifications. Oxidation of methionine was set as a variable modification. A significance threshold of  $p < 0.05$  was applied. The abundances of precursor ions were calculated based on the area of the precursors, determined with Proteome Discoverer 2.5.

## Insoluble fraction assay

Cells were lysed in lysis buffer with protease inhibitor cocktail and 1 mM phenylmethanesulfonyl fluoride for 15 min at 4°C. The lysate was clarified through centrifugation at 20,630 × *g* for 30 min. Then the supernatant was collected as the soluble fraction, and the pellet (containing the insoluble fraction) was washed three times with fresh lysis buffer. The insoluble pellet was suspended in a volume of lysis buffer equal to the soluble fraction volume and then mixed with 6 × SDS sample buffer. The samples were heated to 95°C for 5 min and then sonicated.

## Glycosylation assay

Cells expressing IAPP constructs fused with the glycosylation site of opsin (Pedrazzini *et al.*, 2000) were lysed in 1 × lysis buffer without protease inhibitor, incubated for 15 min on ice, and then centrifuged at 20,630 × *g* for 5 min. The supernatant of each lysate was mixed with 10 × glycoprotein denaturing buffer, heated for 5 min at 95°C, and then incubated with endoglycosidase H or  $\text{H}_2\text{O}$  at 37°C for 10 h. Next, 6 × SDS sample buffer was added to each product; the mixture was heated to 95°C for 5 min and then analyzed through SDS-PAGE and immunoblotting.

## Sucrose gradient fractionation

Cells were lysed in CHAPS(3-[(3-cholamidopropyl)dimethylammonio]-1-propanesulfonate) buffer containing protease inhibitor for 30 min on ice. Then the lysates were centrifuged at 20,630 × *g* for 30 min at 4°C to remove insoluble components; the resulting supernatants were layered on top of a 10–50% discontinuous sucrose gradient and centrifuged at 259,000 × *g* for 90 min at 4°C (CS 150FNX; rotor: S55S [9124280K]; Hitachi, Tokyo, Japan). Eleven 200-µl fractions were collected and mixed with 6 × SDS sample buffer and then analyzed through SDS-PAGE and immunoblotting.

## Immunofluorescence microscopy

Cells were plated on coverslips, fixed in 3.7% formaldehyde in PBS for 15 min, permeabilized with 50 µg/ml digitonin or 0.1% Triton X-100 in PBS for 5 min, and then blocked with 10% newborn bovine serum (NBS) in PBS for 45 min. After blocking, each sample was incubated with the indicated primary antibodies for 1 h. After washing, each sample was incubated with Alexa-647 conjugated anti-mouse or anti-rabbit IgG secondary antibodies (Thermo Fisher Scientific) for

1 h. The stained cells were observed under a confocal laser microscope (FV1000 IX81; Olympus, Tokyo, Japan) using a 100x oil immersion objective lens with a numerical aperture of 1.40. Images were acquired using FV10-ASW 2.1 imaging software.

### Flow cytometry

Cells were trypsinized with EDTA and recovered through detachment from the dish. The cells were passed through a 70- $\mu$ m cell strainer and then resuspended in 10% FBS and 1  $\mu$ g/ml 4',6-diamidino-2-phenylindole (DAPI) in PBS for flow cytometric analysis using a CytoFLEX S flow cytometer equipped with NUV 375-nm (DAPI), 488-nm (GFP), and 561-nm (RFP) lasers (Beckman Coulter, Brea, CA, USA). Dead cells were detected through DAPI staining. In each sample, ten thousand cells were acquired and the RFP/GFP fluorescence ratio was calculated as red fluorescence intensity divided by green fluorescence intensity in RFP-positive cells. The data were processed with Kaluza software (Beckman Coulter).

### Immunoprecipitation

Cells were lysed in lysis buffer with protease inhibitor cocktail and 1 mM phenylmethanesulfonyl fluoride for 15 min at 4°C. The lysate was clarified through centrifugation at 20,630  $\times$  g for 5 min, and the resulting supernatant was collected. A portion of this supernatant was mixed with 6  $\times$  SDS buffer, heated to 95°C for 5 min, and then used as an input. GFP-nanobody Sepharose beads were added to the mixture, which was incubated for 2 h at 4°C. The Sepharose beads were washed four times with lysis buffer before elution with SDS sample buffer. The samples were subsequently separated through SDS-PAGE and analyzed through immunoblotting.

### In vitro protein binding assay

Each DHFR- and small-tag-fusion protein was synthesized using PURE flex2.1 and suspended in 1  $\times$  lysis buffer containing 1% Triton X-100. Substrates for IP and target proteins were mixed at a ratio of 1:3, and the Sepharose beads conjugated to specific antibodies or nanobodies against HA, FLAG, or ALFA were incubated at 4°C for 1 h. The beads were washed four times with 1  $\times$  lysis buffer and 2  $\times$  SDS sample buffer was added. The mixture was then heated to 95°C for 5 min and analyzed using SDS-PAGE and immunoblotting. For analysis of competition for the same cargos, FLAG-tagged products were added at three times the volume of HA-tagged cargos. For analysis of competition for different cargos, P3H4 and  $\delta$ xIAPP were mixed at equal volumes. SDS-PAGE and immunoblotting were performed for analysis.

### RNA extraction, reverse transcription, and quantitative real-time PCR

Total RNA was extracted from cells using ISOGEN II (NIPPON GENE, Tokyo, Japan). Reverse transcription was performed using ReverTra Ace reverse transcription reagents (TOYOBO LIFE SCIENCE, Osaka, Japan). The following gene-specific primer sequences were used: human CCPG1, 5'-TTCTGTGACCCCCACT-GACA-3' (forward) and 5'-TTGGCTGCTTCTCCTTGCT-3' (reverse); human GAPDH, 5'-CCACATCGCTCAGACACCA-3' (forward) and 5'-GGCAACAATCCACTTTACCAGAG-3' (reverse). Relative quantification of gene expression was performed according to the  $2^{-\Delta\Delta CT}$  method. The housekeeping gene GAPDH was used as an internal control to normalize the variability in expression levels.

### ACKNOWLEDGMENTS

We thank Yoshitaka Tanaka (Kyushu University) for the anti-LAMP1 anti-bodies; Takeshi Murata (Chiba University) for cell sorting

support; and Keita Chagi, Eigo Takeda, Yutaro Hama, and members of the Matsuura lab for valuable discussions. This work was supported by JSPS KAKENHI (Grants 19K22413, 20H03249, 22H04634 to E.I., 22J12812 to S.I., 22H04919 to N.M., 18H05270 to H.R.U.), and the JST FOREST Program (Grant JPMJFR204N to E.I.), JST SPRING (Grant JPMJSP2109 to S.I.), JST ERATO (Grants JPMJER1702 to N.M., JPMJER1904 to H.R.U.), Human Frontier Science Program (HFSP) Research Grant Program (Grant RGP0019/2018 to H.R.U.), and Takeda Science Foundation (to E.I.).

### REFERENCES

- Adamson B, Norman TM, Jost M, Cho MY, Nuñez JK, Chen Y, Villalta JE, Gilbert LA, Horlbeck MA, Hein MY, et al. (2016). A multiplexed single-cell CRISPR screening platform enables systematic dissection of the unfolded protein response. *Cell* 167, 1867–1882.e1821.
- An H, Ordureau A, Paulo JA, Shoemaker CJ, Denic V, Harper JW (2019). TEX264 is an endoplasmic reticulum-resident ATG8-interacting protein critical for ER remodeling during nutrient stress. *Mol Cell* 74, 891–908.e810.
- Ast T, Michaelis S, Schuldiner M (2016). The protease Ste24 clears clogged translocons. *Cell* 164, 103–114.
- Bernales S, McDonald KL, Walter P (2006). Autophagy counterbalances endoplasmic reticulum expansion during the unfolded protein response. *PLoS Biol* 4, e23.
- Bhaskara RM, Grumati P, Garcia-Pardo J, Kalayil S, Covarrubias-Pinto A, Chen W, Kudryashev M, Dikic I, Hummer G (2019). Curvature induction and membrane remodeling by FAM134B reticulon homology domain assist selective ER-phagy. *Nat Commun* 10, 2370.
- Blum M, Chang HY, Chuguransky S, Grego T, Kandasamy S, Mitchell A, Nuka G, Paysan-Lafosse T, Qureshi M, Raj S, et al. (2021). The InterPro protein families and domains database: 20 years on. *Nucleic Acids Res* 49, D344–D354.
- Boersema PJ, Raijmakers R, Lemeer S, Mohammed S, Heck AJ (2009). Multiplex peptide stable isotope dimethyl labeling for quantitative proteomics. *Nat Protoc* 4, 484–494.
- Bukau B, Weissman J, Horwich A (2006). Molecular chaperones and protein quality control. *Cell* 125, 443–451.
- Butler AE, Janson J, Bonner-Weir S, Ritzel R, Rizza RA, Butler PC (2003). Beta-cell deficit and increased beta-cell apoptosis in humans with type 2 diabetes. *Diabetes* 52, 102–110.
- Callea F, Brisigotti M, Fabbretti G, Bonino F, Desmet VJ (1992). Hepatic endoplasmic reticulum storage diseases. *Liver* 12, 357–362.
- Chakrabarti A, Chen AW, Varner JD (2011). A review of the mammalian unfolded protein response. *Biotechnol Bioeng* 108, 2777–2793.
- Chen Q, Xiao Y, Chai P, Zheng P, Teng J, Chen J (2019). ATL3 is a tubular ER-phagy receptor for GABARAP-mediated selective autophagy. *Curr Biol* 29, 846–855.e846.
- Chino H, Hatta T, Natsume T, Mizushima N (2019). Intrinsically disordered protein TEX264 mediates ER-phagy. *Mol Cell* 74, 909–921.e906.
- Chino H, Yamasaki A, Ode KL, Ueda HR, Noda NN, Mizushima N (2022). Phosphorylation by casein kinase 2 enhances the interaction between ER-phagy receptor TEX264 and ATG8 proteins. *EMBO Rep*, e54801.
- Chipurupalli S, Ganesan R, Martini G, Mele L, Reggio A, Esposito M, Kannan E, Namasivayam V, Grumati P, Desiderio V, Robinson N (2022). Cancer cells adapt FAM134B/BiP mediated ER-phagy to survive hypoxic stress. *Cell Death Dis* 13, 357.
- De Duve C (1963). The lysosome. *Sci Am* 208, 64–72.
- De Leonibus C, Cinque L, Settembre C (2019). Emerging lysosomal pathways for quality control at the endoplasmic reticulum. *FEBS Lett* 593, 2319–2329.
- Ellgaard L, Helenius A (2003). Quality control in the endoplasmic reticulum. *Nat Rev Mol Cell Biol* 4, 181–191.
- Forrester A, De Leonibus C, Grumati P, Fasana E, Piemontese M, Staiano L, Fregno I, Raimondi A, Marazza A, Bruno G, et al. (2019). A selective ER-phagy exerts procollagen quality control via a calnexin-FAM134B complex. *EMBO J* 38, e99847.
- Fregno I, Fasana E, Bergmann TJ, Raimondi A, Loi M, Soldà T, Galli C, D'Antuono R, Morone D, Danieli A, et al. (2018). ER-to-lysosome-associated degradation of proteasome-resistant ATZ polymers occurs via receptor-mediated vesicular transport. *EMBO J* 37, e99259.
- Fumagalli F, Noack J, Bergmann TJ, Cebollero E, Pisoni GB, Fasana E, Fregno I, Galli C, Loi M, Soldà T, et al. (2016). Translocon component Sec62 acts in endoplasmic reticulum turnover during stress recovery. *Nat Cell Biol* 18, 1173–1184.



- Götzke H, Kilisch M, Martínez-Carranza M, Sograte-Idrissi S, Rajavel A, Schlichthaeerle T, Engels N, Jungmann R, Stenmark P, Opazo F, Frey S (2019). The ALFA-tag is a highly versatile tool for nanobody-based bioscience applications. *Nat Commun* 10, 4403.
- Gruenwald K, Castagnola P, Besio R, Dimori M, Chen Y, Akel NS, Swain FL, Skinner RA, Eyre DR, Gaddy D, et al. (2014). Sc65 is a novel endoplasmic reticulum protein that regulates bone mass homeostasis. *J Bone Miner Res* 29, 666–675.
- Grumati P, Dikic I, Stolz A (2018). ER-phagy at a glance. *J Cell Sci* 131.
- Grumati P, Morozzi G, Hölper S, Mari M, Harwardt MI, Yan R, Müller S, Reggiori F, Heilemann M, Dikic I (2017). Full length RTN3 regulates turnover of tubular endoplasmic reticulum via selective autophagy. *eLife* 6, e25555.
- Hao L, Pang K, Pang H, Zhang J, Zhang Z, He H, Zhou R, Shi Z, Han C (2020). Knockdown of P3H4 inhibits proliferation and invasion of bladder cancer. *Aging (Albany NY)* 12, 2156–2168.
- Hara T, Takamura A, Kishi C, Iemura S, Natsume T, Guan JL, Mizushima N (2008). FIP200, a ULK-interacting protein, is required for autophagosome formation in mammalian cells. *J Cell Biol* 181, 497–510.
- Heard ME, Besio R, Weis M, Rai J, Hudson DM, Dimori M, Zimmerman SM, Kamykowski JA, Hogue WR, Swain FL, et al. (2016). Sc65-null mice provide evidence for a novel endoplasmic reticulum complex regulating collagen lysyl hydroxylation. *PLoS Genet* 12, e1006002.
- Hebert DN, Molinari M (2007). In and out of the ER: protein folding, quality control, degradation, and related human diseases. *Physiol Rev* 87, 1377–1408.
- Hetz C, Zhang K, Kaufman RJ (2020). Mechanisms, regulation and functions of the unfolded protein response. *Nat Rev Mol Cell Biol* 21, 421–438.
- Houck SA, Ren HY, Madden VJ, Bonner JN, Conlin MP, Janovick JA, Conn PM, Cyr DM (2014). Quality control autophagy degrades soluble ERAD-resistant conformers of the misfolded membrane protein GnRHR. *Mol Cell* 54, 166–179.
- Ishida Y, Yamamoto A, Kitamura A, Lamandé SR, Yoshimori T, Bateman JF, Kubota H, Nagata K (2009). Autophagic elimination of misfolded procollagen aggregates in the endoplasmic reticulum as a means of cell protection. *Mol Biol Cell* 20, 2744–2754.
- Iwakura M, Furusawa K, Kokubu T, Ohashi S, Tanaka Y, Shimura Y, Tsuda K (1992). Dihydrofolate reductase as a new "affinity handle." *J Biochem* 111, 37–45.
- Jia W, Pua HH, Li QJ, He YW (2011). Autophagy regulates endoplasmic reticulum homeostasis and calcium mobilization in T lymphocytes. *J Immunol* 186, 1564–1574.
- Jiang X, Wang X, Ding X, Du M, Li B, Weng X, Zhang J, Li L, Tian R, Zhu Q, et al. (2020). FAM134B oligomerization drives endoplasmic reticulum membrane scission for ER-phagy. *EMBO J* 39, e102608.
- Jin X, Zhou H, Song J, Cui H, Luo Y, Jiang H (2021). P3H4 overexpression serves as a prognostic factor in lung adenocarcinoma. *Comput Math Methods Med* 2021, 9971353.
- Jumper J, Evans R, Pritzel A, Green T, Figurnov M, Ronneberger O, Tunyasuvunakool K, Bates R, Židek A, Potapenko A, et al. (2021). Highly accurate protein structure prediction with AlphaFold. *Nature* 596, 583–589.
- Juszkiewicz S, Hegde RS (2018). Quality control of orphaned proteins. *Mol Cell* 71, 443–457.
- Kang SW, Rane NS, Kim SJ, Garrison JL, Taunton J, Hegde RS (2006). Substrate-specific translocational attenuation during ER stress defines a pre-emptive quality control pathway. *Cell* 127, 999–1013.
- Katayama H, Yamamoto A, Mizushima N, Yoshimori T, Miyawaki A (2008). GFP-like proteins stably accumulate in lysosomes. *Cell Struct Funct* 33, 1–12.
- Kayatekin C, Amasino A, Gaglia G, Flannick J, Bonner JM, Fanning S, Narayan P, Barrasa MI, Pincus D, Landgraf D, et al. (2018). Translocon declogger Ste24 protects against IAPP oligomer-induced proteotoxicity. *Cell* 173, 62–73.e69.
- Khaminets A, Heinrich T, Mari M, Grumati P, Huebner AK, Akutsu M, Liebmann L, Stolz A, Nietzsche S, Koch N, et al. (2015). Regulation of endoplasmic reticulum turnover by selective autophagy. *Nature* 522, 354–358.
- Kimura S, Noda T, Yoshimori T (2007). Dissection of the autophagosome maturation process by a novel reporter protein, tandem fluorescently-tagged LC3. *Autophagy* 3, 452–460.
- Kitamura T, Koshino Y, Shibata F, Oki T, Nakajima H, Nosaka T, Kumagai H (2003). Retrovirus-mediated gene transfer and expression cloning: powerful tools in functional genomics. *Exp Hematol* 31, 1007–1014.
- Klionsky DJ, Petroni G, Amaravadi RK, Baehrecke EH, Ballabio A, Boya P, Bravo-San Pedro JM, Cadwell K, Cecconi F, Choi AMK, et al. (2021). Autophagy in major human diseases. *EMBO J* 40, e108863.
- Klöppel G, Löhr M, Habich K, Oberholzer M, Heitz PU (1985). Islet pathology and the pathogenesis of type 1 and type 2 diabetes mellitus revisited. *Surv Synth Pathol Res* 4, 110–125.
- Kostenko EV, Olabisi OO, Sahay S, Rodriguez PL, Whitehead IP (2006). Ccp1, a novel scaffold protein that regulates the activity of the Rho guanine nucleotide exchange factor Dbs. *Mol Cell Biol* 26, 8964–8975.
- Kraft C, Deplazes A, Sohrmann M, Peter M (2008). Mature ribosomes are selectively degraded upon starvation by an autophagy pathway requiring the Ubp3p/Bre5p ubiquitin protease. *Nat Cell Biol* 10, 602–610.
- Lemasters JJ (2005). Selective mitochondrial autophagy, or mitophagy, as a targeted defense against oxidative stress, mitochondrial dysfunction, and aging. *Rejuvenation Res* 8, 3–5.
- Li W, Ye L, Chen Y, Chen P (2018). P3H4 is correlated with clinicopathological features and prognosis in bladder cancer. *World J Surg Oncol* 16, 206.
- Liang CC, Wang C, Peng X, Gan B, Guan JL (2010). Neural-specific deletion of FIP200 leads to cerebellar degeneration caused by increased neuronal death and axon degeneration. *J Biol Chem* 285, 3499–3509.
- Maejima I, Takahashi A, Omori H, Kimura T, Takabatake Y, Saitoh T, Yamamoto A, Hamasaki M, Noda T, Tsaka Y, Yoshimori T (2013). Autophagy sequesters damaged lysosomes to control lysosomal biogenesis and kidney injury. *EMBO J* 32, 2336–2347.
- Melia TJ, Lystad AH, Simonsen A (2020). Autophagosome biogenesis: from membrane growth to closure. *J Cell Biol* 219, e202002085.
- Mercer TJ, Gubas A, Tooze SA (2018). A molecular perspective of mammalian autophagosome biogenesis. *J Biol Chem* 293, 5386–5395.
- Mizushima N, Komatsu M (2011). Autophagy: renovation of cells and tissues. *Cell* 147, 728–741.
- Mizushima N, Yamamoto A, Hatano M, Kobayashi Y, Kabeya Y, Suzuki K, Tokuhisa T, Ohsumi Y, Yoshimori T (2001). Dissection of autophagosome formation using App5-deficient mouse embryonic stem cells. *J Cell Biol* 152, 657–668.
- Mochida K, Nakatogawa H (2022). ER-phagy: selective autophagy of the endoplasmic reticulum. *EMBO Rep* 23, e55192.
- Mochida K, Oikawa Y, Kimura Y, Kirisako H, Hirano H, Ohsumi Y, Nakatogawa H (2015). Receptor-mediated selective autophagy degrades the endoplasmic reticulum and the nucleus. *Nature* 522, 359–362.
- Mochida K, Yamasaki A, Matoba K, Kirisako H, Noda NN, Nakatogawa H (2020). Super-assembly of ER-phagy receptor Atg40 induces local ER remodeling at contacts with forming autophagosomal membranes. *Nat Commun* 11, 3306.
- Molinari M (2021). ER-phagy responses in yeast, plants, and mammalian cells and their crosstalk with UPR and ERAD. *Dev Cell* 56, 949–966.
- Morita K, Hama Y, Izume T, Tamura N, Ueno T, Yamashita Y, Sakamaki Y, Mimura K, Morishita H, Shihoya W, et al. (2018). Genome-wide CRISPR screen identifies. *J Cell Biol* 217, 3817–3828.
- Nakagawa I, Amano A, Mizushima N, Yamamoto A, Yamaguchi H, Kamimoto T, Nara A, Funao J, Nakata M, Tsuda K, et al. (2004). Autophagy defends cells against invading group A *Streptococcus*. *Science* 306, 1037–1040.
- Ni M, Lee AS (2007). ER chaperones in mammalian development and human diseases. *FEBS Lett* 581, 3641–3651.
- Nthiga TM, Kumar Shrestha B, Sjøttem E, Bruun JA, Bowitz Larsen K, Bhujabal Z, Lamark T, Johansen T (2020). CALCOCO1 acts with VAMP-associated proteins to mediate ER-phagy. *EMBO J* 39, e103649.
- Ochs RL, Stein TW, Chan EK, Ruutu M, Tan EM (1996). cDNA cloning and characterization of a novel nucleolar protein. *Mol Biol Cell* 7, 1015–1024.
- Øverbye A, Fengsrud M, Seglen PO (2007). Proteomic analysis of membrane-associated proteins from rat liver autophagosomes. *Autophagy* 3, 300–322.
- Pedrazzini E, Villa A, Longhi R, Bulbarelli A, Borgese N (2000). Mechanism of residence of cytochrome b(5), a tail-anchored protein, in the endoplasmic reticulum. *J Cell Biol* 148, 899–914.
- Pengo N, Scolari M, Oliva L, Milan E, Mainoldi F, Raimondi A, Fagioli C, Merlini A, Mariani E, Pasqualetto E, et al. (2013). Plasma cells require autophagy for sustainable immunoglobulin production. *Nat Immunol* 14, 298–305.
- Rappsilber J, Mann M, Ishihama Y (2007). Protocol for micro-purification, enrichment, pre-fractionation and storage of peptides for proteomics using StageTips. *Nat Protoc* 2, 1896–1906.
- Ruggiano A, Foresti O, Carvalho P (2014). Quality control: ER-associated degradation: protein quality control and beyond. *J Cell Biol* 204, 869–879.
- Rutishauser J, Spiess M (2002). Endoplasmic reticulum storage diseases. *Swiss Med Wkly* 132, 211–222.

- Saitoh T, Fujita N, Hayashi T, Takahara K, Satoh T, Lee H, Matsunaga K, Kageyama S, Omori H, Noda T, *et al.* (2009). Atg9a controls dsDNA-driven dynamic translocation of STING and the innate immune response. *Proc Natl Acad Sci USA* 106, 20842–20846.
- Schröder M, Kaufman RJ (2005). ER stress and the unfolded protein response. *Mutat Res* 569, 29–63.
- Shimizu Y, Inoue A, Tomari Y, Suzuki T, Yokogawa T, Nishikawa K, Ueda T (2001). Cell-free translation reconstituted with purified components. *Nat Biotechnol* 19, 751–755.
- Shimizu Y, Kanamori T, Ueda T (2005). Protein synthesis by pure translation systems. *Methods* 36, 299–304.
- Singh R, Kaushik S, Wang Y, Xiang Y, Novak I, Komatsu M, Tanaka K, Cuervo AM, Czaja MJ (2009). Autophagy regulates lipid metabolism. *Nature* 458, 1131–1135.
- Smith M, Wilkinson S (2017). ER homeostasis and autophagy. *Essays Biochem* 61, 625–635.
- Smith MD, Harley ME, Kemp AJ, Wills J, Lee M, Arends M, von Kriegsheim A, Behrends C, Wilkinson S (2018). CCPG1 is a non-canonical autophagy cargo receptor essential for ER-phagy and pancreatic ER proteostasis. *Dev Cell* 44, 217–232.e211.
- Stephani M, Picchianti L, Gajic A, Beveridge R, Skarwan E, Sanchez de Medina Hernandez V, Mohseni A, Clavel M, Zeng Y, Naumann C, *et al.* (2020). A cross-kingdom conserved ER-phagy receptor maintains endoplasmic reticulum homeostasis during stress. *Elife* 9, e58396.
- Stolz A, Ernst A, Dikic I (2014). Cargo recognition and trafficking in selective autophagy. *Nat Cell Biol* 16, 495–501.
- Sun J, Wang W, Zheng H (2022). ROOT HAIR DEFECTIVE3 is a receptor for selective autophagy of the endoplasmic reticulum in Arabidopsis. *Front Plant Sci* 13, 817251.
- Tian X, Jin RU, Bredemeyer AJ, Oates EJ, Błazewska KM, McKenna CE, Mills JC (2010). RAB26 and RAB3D are direct transcriptional targets of MIST1 that regulate exocrine granule maturation. *Mol Cell Biol* 30, 1269–1284.
- Turco E, Witt M, Abert C, Bock-Bierbaum T, Su MY, Trapannone R, Sztacho M, Danieli A, Shi X, Zaffagnini G, *et al.* (2019). FIP200 claw domain binding to p62 promotes autophagosome formation at ubiquitin condensates. *Mol Cell* 74, 330–346.e311.
- Uhlén M, Fagerberg L, Hallström BM, Lindskog C, Oksvold P, Mardinoglu A, Sivertsson Å, Kampf C, Sjöstedt E, Asplund A, *et al.* (2015). Proteomics. Tissue-based map of the human proteome. *Science* 347, 1260419.
- Varadi M, Anyango S, Deshpande M, Nair S, Natassia C, Yordanova G, Yuan D, Stroe O, Wood G, Laydon A, *et al.* (2022). AlphaFold protein structure database: massively expanding the structural coverage of protein-sequence space with high-accuracy models. *Nucleic Acids Res* 50, D439–D444.
- Webb JL, Ravikumar B, Atkins J, Skepper JN, Rubinsztein DC (2003). Alpha-synuclein is degraded by both autophagy and the proteasome. *J Biol Chem* 278, 25009–25013.
- Wilfling F, Lee CW, Erdmann PS, Zheng Y, Sherpa D, Jentsch S, Pfander B, Schulman BA, Baumeister W (2020). A selective autophagy pathway for phase-separated endocytic protein deposits. *Mol Cell* 80, 764–778.e767.
- Wilkinson S (2020). Emerging principles of selective ER autophagy. *J Molecular Biol* 432, 185–205.
- Yamasaki A, Alam JM, Noshiro D, Hirata E, Fujioka Y, Suzuki K, Ohsumi Y, Noda NN (2020). Liquidity is a critical determinant for selective autophagy of protein condensates. *Mol Cell* 77, 1163–1175.e1169.
- Yim WW, Yamamoto H, Mizushima N (2022). A pulse-chasable reporter processing assay for mammalian autophagic flux with HaloTag. *Elife* 11, e78923.
- Yoshii SR, Kuma A, Akashi T, Hara T, Yamamoto A, Kurikawa Y, Itakura E, Tsukamoto S, Shitara H, Eishi Y, Mizushima N (2016). Systemic analysis of Atg5-null mice rescued from neonatal lethality by transgenic ATG5 expression in neurons. *Dev Cell* 39, 116–130.
- Zhao D, Zou CX, Liu XM, Jiang ZD, Yu ZQ, Suo F, Du TY, Dong MQ, He W, Du LL (2020). A UPR-induced soluble ER-phagy receptor acts with VAPs to confer ER stress resistance. *Mol Cell* 79, 963–977.e963.